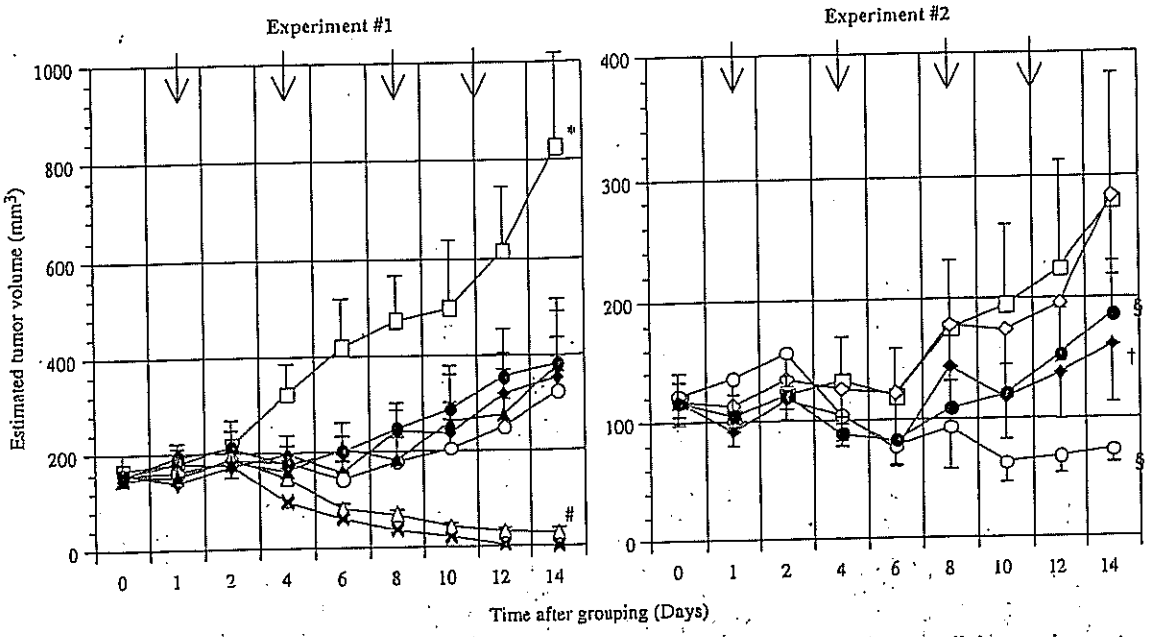

Fig. 4. Time-course change in estimated tumor volumes of subcutaneously transplanted human hepatocellular carcinoma tumors in nude mice. The mice received a subcutaneous injection of 640 (♦), 6400 (○), 64 000 (△), or 640 000 (✱) IU of pegylated IFN-α2b (PEG-IFN-α2b), or 6400 (●) or 64 000 (▲) IU of IFN-α2b, or medium alone (Control) (□) in Experiment #1, and of 640 (♦) or 6400 (○) IU of PEG-IFN-α2b, 640 (◇) or 6400 (●) IU of IFN-α2b, or medium alone (Control) (□) in Experiment #2, twice a week for two consecutive weeks. The arrows show the days of injection. *$P<0.001$, vs the other groups. #$P<0.0001$, vs IFN-α2b (64 000 IU). †$P<0.05$, vs control or IFN-α2b (640 IU). §$P<0.05$, vs Control. The experiments were repeated twice, and almost identical results were obtained. The figures represent average ± SE.

Table 2. Treatment of human HCC tumors subcutaneously transplanted in nude mice

Treatment group*	Number	Tumor weight (g)	Body weight (g)†
Experiment #1			
Control	8	0.436 ± 0.07‡	19.2 ± 0.6††
PEG-IFN-α2b (640 IU)	9	0.237 ± 0.05§	19.4 ± 0.4
PEG-IFN-α2b (6400 IU)	9	0.180 ± 0.03¶	19.9 ± 0.3
IFN-α2b (6400 IU)	6	0.259 ± 0.06§	19.4 ± 0.7
PEG-IFN-α2b (64 000 IU)	9	0.016 ± 0.01 ‖ ,#	19.0 ± 0.6
IFN-α2b (64 000 IU)	7	0.221 ± 0.06§	19.1 ± 0.5
PEG-IFN-α2b (640 000 IU)	9	0.0 ‖	19.6 ± 0.3
Experiment #2			
Control	8	0.160 ± 0.04	20.6 ± 0.5††
PEG-IFN-α2b (640 IU)	8	0.097 ± 0.02	20.1 ± 0.4
IFN-α2b (640 IU)	8	0.168 ± 0.03	20.7 ± 0.4
PEG-IFN-α2b (6400 IU)	7	0.050 ± 0.02¶	21.0 ± 0.3
IFN-α2b (6400 IU)	8	0.131 ± 0.03**	21.1 ± 0.3

*Cultured HAK-1B cells (1.0×10^7) were subcutaneously transplanted into nude mice. Five to seven days later when the largest diameter of the tumor reached approximately 5–10 mm, mice in each group were treated with twice per week sc injections of PEG-IFN-α2b, IFN-α2b, or culture medium. All mice were sacrificed on the 15th day. †Body weight on the 14th day. ‡Mean ± SE. §$P<0.05$ vs control. ¶$P<0.01$ vs control. ‖ $P<0.001$ vs control. #$P<0.01$ vs IFN-α2b (64 000 IU). **$P<0.03$ vs PEG-IFN-α2b (6400 IU). ††not significant vs the other groups. HCC, hepatocellular carcinoma; PEG-IFN-α2b, pegylated IFN-α2b.

PEG- and non-PEG-IFN-α2b ($P<0.05$, Fig 4). The tumors of the mice that received 6400 IU of PEG-IFN-α2b tended to be smaller in volume in both Experiments #1 and #2 ($P=0.068$ and 0.064, respectively), and the tumor was significantly lower in weight than that of IFN-α2b in Experiment #2 ($P<0.03$). At the end of the experiments, the estimated tumor volume in the mice that received 640 IU of PEG-IFN-α2b (3.2×10^4 IU/kg, about 1/3 of the clinical dose 9.6×10^4 IU/kg) in Experiments #1 and #2 became 42% and 58% of the Control, respectively. In the mice that received 640 000 IU of PEG-IFN-α2b, the tumors disappeared on the 14th day. PEG-IFN-α2b administration did not affect the body weight of the mice (Table 2).

Histological examination of the HAK-1B tumor specimens stained with HE revealed that the numbers of apoptotic cells in the mice treated with PEG-IFN-α2b (640–64 000 IU) or IFN-α2b (64 000 IU) were significantly higher than that of the Control, and the number increased dose dependently (Fig. 5A–C; Table 3). Immunostaining of vimentin fragment (V1) that is a marker for caspase-9 activation showed a positive reaction in the cytoplasm of the apoptotic cells (Fig. 5D).

No significant difference was observed in the number of blood vessels per unit area of the HAK-1B tumor between the Control and the PEG-IFN-α2b or IFN-α2b group (Table 3).

Immunohistochemical examination of BrdU uptake in HAK-1B tumors revealed that the BrdU labeling index was significantly higher in the Control than in the 6400 IU PEG-IFN-α2b or IFN-α2b groups (Fig. 5E, Table 3).

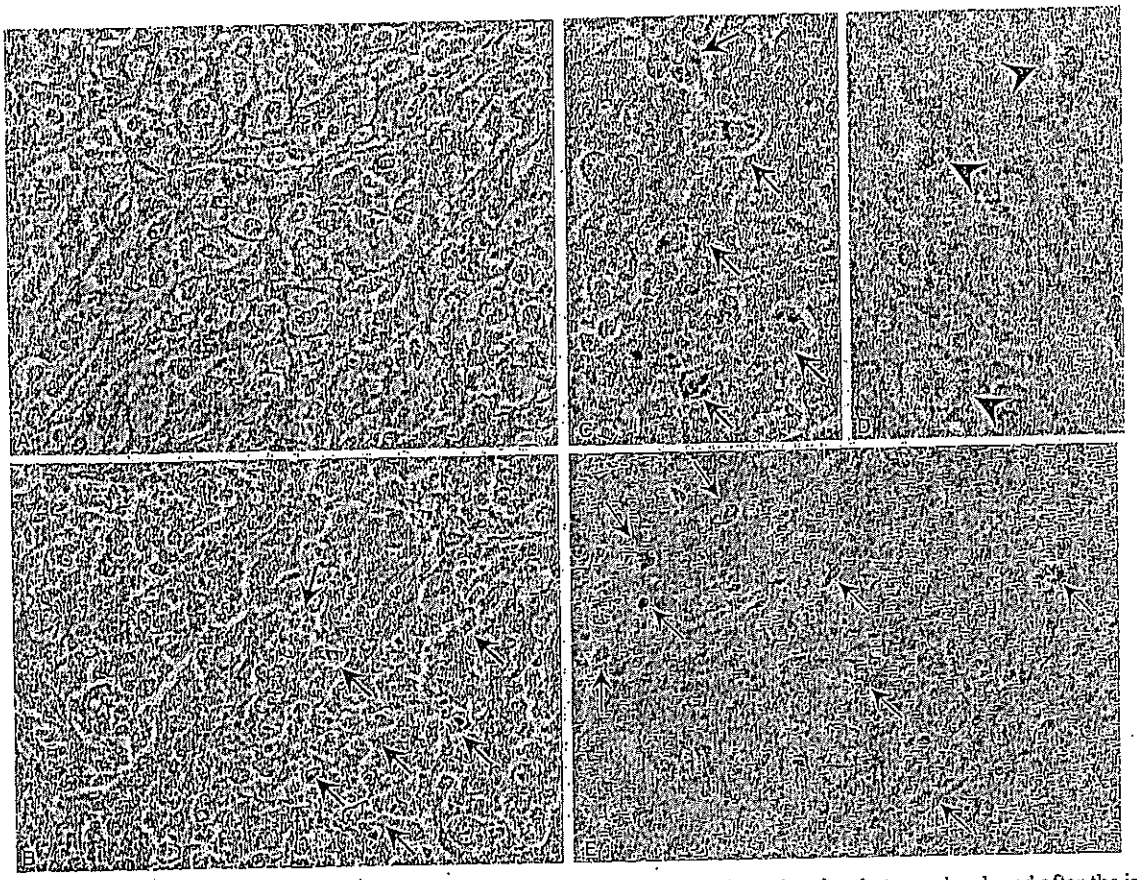

Fig. 5. Photomicrograph of subcutaneous human hepatocellular carcinoma tumor in nude mice that was developed after the injection of HAK-1B cells. (A) A control mouse that received culture medium alone. The tumor shows a thick trabecular arrangement of tumor cells and a sinusoid-like structure in the stroma. (B) A mouse that received a sc injection of 6400 IU pegylated IFN-α2b. There are many apoptotic tumor-cells (arrows, hematoxylin–eosin staining, × 200). (C) Higher magnification of B. It clearly shows apoptotic tumor cells characterized by shrinkage and eosinophilic change in the cytoplasm, chromatin condensation and/or fragmentation of nuclei (hematoxylin–eosin staining, × 400). (D) Immunostaining of vimentin fragment (V1). Positive reactions (red pigments) are shown in the shrunken cytoplasm of apoptotic cells as noted in C (counterstained with Mayer's hematoxylin, × 400). (E) Immunostaining of bromodeoxyuridine (BrdU). Many BrdU-positive cells (brown nuclear pigments) were found in a tumor of a control mouse (counterstained with Mayer's hematoxylin, × 200).

Table 3. Numbers of apoptotic cells, artery-like blood vessels, and BrdU-positive cells, and expression of IFNAR-2 subunit in human HCC tumors subcutaneously transplanted in nude mice

Treatment group*	Apoptosis†	Blood vessel‡	BrdU L.I.§	IFNAR-2¶
Experiment #1				
Control	21.3 ± 1.8 ‖	1.16 ± 0.20 ‖ ,**	15.5 ± 1.2 ‖	0.676 ± 0.10 ‖
PEG-IFN-α2b (640 IU)	28.4 ± 1.9#	1.04 ± 0.15	16.6 ± 3.1	0.410 ± 0.07#
PEG-IFN-α2b (6400 IU)	34.3 ± 5.0#	1.20 ± 0.19	10.2 ± 1.1#	0.451 ± 0.11
IFN-α2b (6400 IU)	24.0 ± 3.0	1.13 ± 0.16	9.4 ± 1.1#	0.656 ± 0.12
PEG-IFN-α2b (64 000 IU)	34.3 ± 5.3#	1.43 ± 0.39	ND	0.061 ± 0.06††
IFN-α2b (64 000 IU)	27.5 ± 2.5#	0.92 ± 0.20	10.6 ± 3.0	0.607 ± 0.11
PEG-IFN-α2b (640 000 IU)	ND	ND	ND	ND

*Cultured HAK-1B cells (1.0×10^7) were subcutaneously transplanted into nude mice. Five to seven days later when the largest diameter of the tumor reached approximately 5–10 mm, mice in each group were treated with twice per week sc injections of PEG-IFN-α2b, IFN-α2b, or culture medium. All mice were sacrificed on the 15th day. †The number of apoptotic cells was counted in ten 0.25 mm^2 areas in each section, and the average number per area in each group was obtained. ‡The number of the blood vessels in the tumor nodule was counted on each section, and the average number per area in each group was obtained. §The number of BrdU-positive cells was counted in ten 0.25 mm^2 areas in each section, and the average number per area in each group was obtained as the labeling index. ¶Values are expressed as pg/15 μg protein. ‖ Mean ± SE. #$P < 0.05$, vs control. **Not significant, vs the other groups. ††Not significant ($P = 0.068$) vs control. This is partly because only 2 samples were available for IFNAR-2 analysis in this group. BrdU, bromodeoxyuridine; IFNAR-2, IFN-α receptor-2; HCC, hepatocellular carcinoma; ND, not done; PEG-IFN-α2b, pegylated IFN-α2b.

The expression of the IFNAR-2 subunit tended to decrease in the PEG-IFN-α2b groups, and a significant difference was observed between the Control and the 640 IU PEG-IFN-α2b group ($P < 0.05$).

Discussion

PEG-IFN-α2b induced a time-dependent antiproliferative effect in 10 cell lines in contact with 4096 IU/ml of PEG-IFN-α2b for 24–96 h and a dose-dependent antiproliferative effect in nine cell lines *in vitro* in the range of 16 and 4096 IU/ml. On an antiviral unit basis, the antiproliferative activity of PEG-IFN-α2b was not significantly different from that of non-PEG-IFN-α2b *in vitro* based on IC50 values. Compared with BALL-1 IFN-α that consists of the α2 subtype (about 75%) and the α8 subtype (25%) or with IFN-αCon1, both PEG-IFN-α2b and IFN-α2b showed low antiproliferative activity in terms of relative viable cell number and IC50 (11, 12). This is consistent with our recent finding, i.e., that the antiproliferative activity of the IFN-α2 subtype *in vitro* is relatively weak compared with other IFN-α subtypes such as α5, α10 and α8 (32). As a mechanism of antiproliferation, apoptosis induction was observed in 9 cell lines that received 1000 IU/ml of PEG-IFN-α2b (morphological changes occurred in 10 cell lines with 4096 IU/ml). IFN-αCon1 that possesses the most potent antiproliferative effect among the three IFN-α preparations induced apoptosis in all 13 HCC cell lines at a similar concentration (12). The four cell lines (HAK-2, HAK-3, HAK-4, and KMCH-2) in which PEG-IFN-α2b did not induce a dose-dependent antiproliferative effect showed the highest IC50 values (> 100 000 IU/ml) to IFN-α2 subtype among the 13 cell lines (32) and showed resistance to PEG-IFN-α2b-mediated apoptosis (HAK-2, HAK-3, and KMCH-2) and/or low cell surface IFNAR-2 expression (HAK-3, HAK-4, and KMCH-2) (11).

When IFN-α binds to its receptors, the IFN-receptor-complexes are internalized and degradated intracellularly (33, 34). It was demonstrated that IFN-α down-regulates type I IFN receptors in peripheral blood mononuclear cells (PBMC, (35–37)). Nakajima et al. (36) reported that the number of IFN receptors on PBMC in patients with chronic hepatitis B decreased to about 50% of the baseline with a fivefold increase in 2′,5′-oligoadenylate synthetase activity when the patients were treated with IFN for 2 or 4 weeks. To date, however, there have been no studies on the down-regulation of IFN receptors and its relationship with the antiproliferative effects of IFN-α in liver cancer cells. Human type I IFN receptor consists of two subunits, IFNAR-1 and IFNAR-2. IFNAR-2 is the binding subunit and is more important than IFNAR-1 for the expression of IFN activity (3, 38, 39). Therefore, the current study chronologically examined the relationship between the antiproliferative effect and the expression of the IFNAR-2 subunit in HAK-1B cells up to 240 h after the addition of PEG-IFN-α2b. We chose HAK-1B for this study because this cell line expresses the highest IFNAR-2 subunit expression among the 13 liver cancer cell lines (11) and because this cell line was also selected for the *in vivo* experiment, allowing comparison of results in the *in vitro* setting with those *in vivo*. The expression of IFNAR-2 subunit was significantly down-regulated at 3 h compared with the Control and then significantly up-regulated at 48 h. Expression then decreased in a time-dependent manner after 72 h, and the viable cell number continuously decreased with time. The down-regulation of IFNAR-2 was the specific change because another cell surface protein, i.e., EGF receptor, was not down-regulated at 240 h compared with Control. Therefore, at least for the HCC cell line, HAK-1B, in an *in vitro* setting, the IFNAR-2 subunit is down-regulated but an efficient antiproliferative effect is induced with continuous contact with PEG-IFN-α2b. Lau et al. (35) studied the binding characteristics of IFN-α to PBMC in patients with chronic hepatitis B virus infection and reported a possible increase in binding affinity of the remaining receptors as a reason for the continuous effects of IFN-α in long-term IFN therapy that reduces the number of IFN-α receptors. On the other hand, Dooley et al. (40) reported a decrease in binding affinity. Therefore, this point also needs to be further studied on HAK-1B and other HCC cell lines.

We then examined the *in vivo* antitumor effects of PEG-IFN-α2b on mice. Twice-a-week administration of PEG-IFN-α2b dose-dependently suppressed the growth of sc transplanted human HCC. The growth was effectively suppressed even at 1/3 of the clinical dose in patients with chronic hepatitis C, and the tumor size was reduced to 42–58% of the Control. This antiproliferative effect was equivalent to the effect of a consecutive 14-day administration of an approximately 1.3 times larger clinical dose of IFN-αCon1 (12). The antiproliferative effect of PEG-IFN-α2b *in vitro* is lower than IFN-αCon1; therefore, our *in vivo* finding would be understood as the serum half-time of IFN-α2b becoming longer due to pegylation, then PEG-IFN-α2b at a high concentrations remaining in the serum for a long time to affect tumor cells, resulting in much stronger antitumor effects. This consideration is also supported by our results, i.e., PEG-IFN-α2b and IFN-α2b *in vitro* presented the same antiproliferative effects; however, *in vivo*, IFN-α2b presented significantly weaker antitumor

effects than PEG-IFN-α2b. In addition, IFNAR-2 expression in the tumor of mice decreased, particularly in mice that received PEG-IFN-α2b. This was considered to be due to IFNAR-2 expression being down-regulated as a result of the long-term continuous action of PEG-IFN-α2b, and this is consistent with the *in vitro* findings. The above indicates that even if IFNAR-2 expression is down-regulated, antitumor effect does not decrease but, in fact, increases due to continuous action. In contrast, Krepler et al. (41) compared antitumor effects of PEG-IFN-α2a and non-PEG-IFN-α2a in a human melanoma SCID mouse xenotransplantation model and found no significant differences in tumor growth inhibition. We presume that this opposite result is attributable to the difference in the experimental conditions. For example, in their study, mice received extremely high doses of PEG- and non-PEG-IFN-α2a, i.e., mice received 900 μg of PEG-IFN-α2a (45 000 μg/kg) that is five or 10 times larger than the clinical dose for chronic hepatitis C patients (90–180 μg/body, 1.8–3.6 μg/kg). In addition, it is not clear whether the amounts of PEG- and non-PEG-IFN-α2a administrated to mice were equivalent in antiproliferative effects on the melanoma cells *in vitro*.

The induction of apoptosis is known as a mechanism of the *in vivo* antiproliferation activity of PEG-IFN-α2b. However, the induction of S-phase arrest that was observed *in vitro* was not clear *in vivo* in terms of the labeling index of BrdU. This was the same as the finding on the mechanism of the antiproliferation activity of IFN-αCon1 in mouse tumor (12). It is surmized that apoptosis holds the dominant position over the S-phase arrest when tumor cells *in vivo* were treated with IFN-α for 2 weeks. This point should be further investigated. Antiangiogenesis activity is one of the biological effects of IFN-α, and the administration of IFN-α to patients with vascular tumors, e.g., Kaposi sarcoma, results in the significant regression of tumor lesions (1, 4). IFN administration suppresses the growth of human tumor that was transplanted to mice through an antiangiogenesis effect (12, 31, 42–45). Tedjarati et al. (44) found that once per week injection of 7000 IU of PEG-IFN-α2b into nude mice bearing ip growing human ovarian carcinoma cells inhibited angiogenesis and tumor growth and that PEG-IFN-α2b administered at higher or lower doses was less effective. In our current study, however, significant antiangiogenesis effect was not observed at any dose. In another study that we conducted examining a consecutive 14-day administration of 5000 IU/mouse/day of BALL-1 IFN-α to mice that had subcutaneous transplantation of HAK-1B tumor, a slight increase in the number of blood vessels and an increase of the three angiogenesis factors were observed (46). On the other hand, another study that used 0.01 or 0.1 μg/mouse of IFN-αCon1 showed a significant decrease in the number of blood vessels (12). Further studies are necessary both *in vitro* and *in vivo* with various IFNs such as IFN-α and IFN-β to clarify whether the antiangiogenesis effects are attributable to the type of IFN. In addition, more studies are also needed to investigate the mechanism of antiproliferative effects including antiangiogenesis, the expression of IFNAR-2 and its relationship to antiproliferative effects using other HCC cells.

In the HCC cell line HAK-1B, continuous contact with PEG-IFN-α2b induced the down-regulation of IFNAR-2 and a potent antiproliferative effect that is stronger than the effects of non-PEG-IFN-α2b. The antitumor effect of PEG-IFN-α2b was expressed at approximately 1/3 of the clinical dose, and this suggests that PEG-IFN-α2b administration to patients with chronic hepatitis C would be effective in the prevention of hepatocarcinogenesis and the recurrence of HCC.

Acknowledgements

We thank Ms. Akemi Fujiyoshi and Dr. Akiko Takayama for their assistance in our experiments. This study was supported in part by the Sarah Cousins Memorial Fund, Boston, Massachusetts, and by a Grant-in-Aid from the Ministry of Health, Labor and Welfare of Japan (#17200501).

References

1. Stark G R, Kerr I M, Williams B R, Silverman R H, Schreiber R D. How cells respond to interferons. Annu Rev Biochem 1998; 67: 227–64.
2. Xu D, Erickson S, Szeps M, et al. Interferon α down-regulates telomerase reverse transcriptase and telomerase activity in human malignant and nonmalignant hematopoietic cells. Blood 2000; 96: 4313–8.
3. Pestka S, Langer J A, Zoon K C, Samuel C E. Interferons and their actions. Annu Rev Biochem 1987; 56: 727–77.
4. Gutterman J U. Cytokine therapeutics: lessons from interferon α. Proc Natl Acad Sci USA 1994; 91: 1198–205.
5. Ikeda K, Saitoh S, Arase Y, et al. Effect of interferon therapy on hepatocellular carcinogenesis in patients with chronic hepatitis type C: a long-term observation study of 1643 patients using statistical bias correction with proportional hazard analysis. Hepatology 1999; 29: 1124–30.
6. Ikeda K, Arase Y, Saitoh S, et al. Interferon beta prevents recurrence of hepatocellular carcinoma after complete resection or ablation of the primary tumor-A prospective randomized study of hepatitis C virus-related liver cancer. Hepatology 2000; 32: 228–32.
7. Mazzella G, Accogli E, Sottili S, et al. Alpha interferon treatment may prevent hepatocellular carcinoma in HCV-related liver cirrhosis. J Hepatol 1996; 24: 141–7.

8. Nishiguchi S, Kuroki T, Nakatani S, et al. Randomised trial of effects of interferon-α on incidence of hepatocellular carcinoma in chronic active hepatitis C with cirrhosis. Lancet 1995; 346: 1051–5.
9. Nishiguchi S, Tamori A, Kubo S. Effect of long-term postoperative interferon therapy on intrahepatic recurrence and survival rate after resection of hepatitis C virus-related hepatocellular carcinoma. Intervirology 2005; 48: 71–5.
10. Sakaguchi Y, Kudo M, Fukunaga T, Minami Y, Chung H, Kawasaki T. Low-dose, long-term, intermittent interferon-alpha-2b therapy after radical treatment by radiofrequency ablation delays clinical recurrence in patients with hepatitis C virus-related hepatocellular carcinoma. Intervirology 2005; 48: 64–70.
11. Yano H, Iemura A, Haramaki M, et al. Interferon alfa receptor expression and growth inhibition by interferon alfa in human liver cancer cell lines. Hepatology 1999; 29: 1708–17.
12. Hisaka T, Yano H, Ogasawara S, et al. Interferon-αCon1 suppresses proliferation of liver cancer cell lines *in vitro* and *in vivo*. J Hepatol 2004; 41: 782–9.
13. Negrier S, Escudier B, Lasset C, et al. Recombinant human interleukin-2, recombinant human interferon alfa-2a, or both in metastatic renal-cell carcinoma. Groupe Francais d'Immunotherapie. N Engl J Med 1998; 338: 1272–8.
14. Sakon M, Nagano H, Dono K, et al. Combined intraarterial 5-fluorouracil and subcutaneous interferon-alpha therapy for advanced hepatocellular carcinoma with tumor thrombi in the major portal branches. Cancer 2002; 94: 435–42.
15. Baker D E. Pegylated interferon plus ribavirin for the treatment of chronic hepatitis C. Rev Gastroenterol Disord 2003; 3: 93–109.
16. Reddy K R, Wright T L, Pockros P J, et al. Efficacy and safety of pegylated (40-kd) interferon α-2a compared with interferon α-2a in noncirrhotic patients with chronic hepatitis C. Hepatology 2001; 33: 433–8.
17. Lindsay K L, Trepo C, Heintges T, et al. A randomized, double-blind trial comparing pegylated interferon alfa-2b to interferon alfa-2b as initial treatment for chronic hepatitis C. Hepatology 2001; 34: 395–403.
18. Craxi A, Licata A. Clinical trial results of peginterferons in combination with ribavirin. Semin Liver Dis 2003; 23(Suppl. 1): 35–46.
19. Lee S D, Yu M L, Cheng P N, et al. Comparison of a 6-month course peginterferon α-2b plus ribavirin and interferon α-2b plus ribavirin in treating Chinese patients with chronic hepatitis C in Taiwan. J Viral Hepatol 2005; 12: 283–91.
20. Bruno S, Camma C, Di Marco V, et al. Peginterferon alfa-2b plus ribavirin for naive patients with genotype 1 chronic hepatitis C: a randomized controlled trial. J Hepatol 2004; 41: 474–81.
21. Utsunomiya I, Iemura A, Yano H, Akiba J, Kojiro M. Establishment and characterization of a new human hepatocellular carcinoma cell line, HAK-3, and its response to growth factors. Int J Oncol 1999; 15: 669–75.
22. Murakami T. Establishment and characterization of human hepatoma cell line (KIM-1). Acta Hepatol Jpn 1984; 25: 532–9.
23. Murakami T, Maruiwa M, Fukuda K, Kojiro M, Tanaka M, Tanikawa K. Characterization of a new human hepatoma cell line (KYN-3) derived from the ascites of the hepatoma patient [Abstract]. Jpn J Cancer Res 1988;Proceedings of the Japanese Cancer Association: 292.
24. Murakami T, Yano H, Maruiwa M, Sugihara S, Kojiro M. Establishment and characterization of a human combined hepatocholangiocarcinoma cell line and its heterologous transplantation in nude mice. Hepatology 1987; 7: 551–6.
25. Haramaki M, Yano H, Iemura A, et al. A new human hepatocellular carcinoma cell line (HAK-2) forms various structures in collagen gel matrices. Hum Cell 1997; 10: 183–92.
26. Yano H, Iemura A, Fukuda K, Mizoguchi A, Haramaki M, Kojiro M. Establishment of two distinct human hepatocellular carcinoma cell lines from a single nodule showing clonal dedifferentiation of cancer cells. Hepatology 1993; 18: 320–7.
27. Yano H, Iemura A, Haramaki M, et al. A human combined hepatocellular and cholangiocarcinoma cell line (KMCH-2) that shows the features of hepatocellular carcinoma or cholangiocarcinoma under different growth conditions. J Hepatol 1996; 24: 413–22.
28. Yano H, Kojiro M, Nakashima T. A new human hepatocellular carcinoma cell line (KYN-1) with a transformation to adenocarcinoma. In Vitro Cell Dev Biol 1986; 22: 637–46.
29. Yano H, Maruiwa M, Murakami T, et al. A new human pleomorphic hepatocellular carcinoma cell line, KYN-2. Acta Pathol Jpn 1988; 38: 953–66.
30. Nakanishi K, Maruyama M, Shibata T, Morishima N. Identification of a caspase-9 substrate and detection of its cleavage in programmed cell death during mouse development. J Biol Chem 2001; 276: 41237–44.
31. Takemoto Y, Yano H, Momosaki S, et al. Antiproliferative effects of interferon-αCon1 on ovarian clear cell adenocarcinoma *in vitro* and *in vivo*. Clin Cancer Res 2004; 10: 7418–26.
32. Yano H, Yanai Y, Momosaki S, et al. Growth inhibitory effects of interferon-α subtypes vary according to human liver cancer cell lines. J Gastroenterol Hepatol 2006, in press.
33. Evans T, Secher D. Kinetics of internalisation and degradation of surface-bound interferon in human lymphoblastoid cells. EMBO J 1984; 3: 2975–8.
34. Zoon K C, Zur Nedden D, Hu R, Arnheiter H. Analysis of the steady state binding, internalization, and degradation of human interferon-α2. J Biol Chem 1986; 261: 4993–6.
35. Lau J Y, Sheron N, Morris A G, Bomford A B, Alexander G J, Williams R. Interferon-α receptor expression and regulation in chronic hepatitis B virus infection. Hepatology 1991; 13: 332–8.
36. Nakajima S, Kuroki T, Shintani M, et al. Changes in interferon receptors on peripheral blood mononuclear cells from patients with chronic hepatitis B being treated with interferon. Hepatology 1990; 12: 1261–5.
37. Tochizawa S, Akamatsu S, Sugiyama Y, et al. A flow cytometric method for determination of the interferon receptor IFNAR2 subunit in peripheral blood leukocyte subsets. J Pharmacol Toxicol Methods 2004; 50: 59–66.
38. Lutfalla G, Holland S J, Cinato E, et al. Mutant U5A cells are complemented by an interferon-αβ receptor subunit generated by alternative processing of a new member of a cytokine receptor gene cluster. EMBO J 1995; 14: 5100–8.
39. Domanski P, Witte M, Kellum M, et al. Cloning and expression of a long form of the β subunit of the interferon αβ receptor that is required for signaling. J Biol Chem 1995; 270: 21606–11.
40. Dooley J S, Vergalla J, Hoofnagle J H, Zoon K C, Munson P J, Jones E A. Specific binding of human alpha interferon to high-affinity cell-surface binding sites on peripheral blood mononuclear cells. J Lab Clin Med 1989; 113: 623–31.
41. Krepler C, Certa U, Wacheck V, Jansen B, Wolff K, Pehamberger H. Pegylated and conventional interferon-α

induce comparable transcriptional responses and inhibition of tumor growth in a human melanoma SCID mouse xenotransplantation model. J Invest Dermatol 2004; 123: 664–9.
42. Dinney C P, Bielenberg D R, Perrotte P, et al. Inhibition of basic fibroblast growth factor expression, angiogenesis, and growth of human bladder carcinoma in mice by systemic interferon-alpha administration. Cancer Res 1998; 58: 808–14.
43. Hong Y K, Chung D S, Joe Y A, et al. Efficient inhibition of *in vivo* human malignant glioma growth and angiogenesis by interferon-beta treatment at early stage of tumor development. Clin Cancer Res 2000; 6: 3354–60.
44. Tedjarati S, Baker C H, Apte S, et al. Synergistic therapy of human ovarian carcinoma implanted orthotopically in nude mice by optimal biological dose of pegylated interferon alpha combined with paclitaxel. Clin Cancer Res 2002; 8: 2413–22.
45. Singh R K, Gutman M, Llansa N, Fidler I J. Interferon-beta prevents the upregulation of interleukin-8 expression in human melanoma cells. J Interferon Cytokine Res 1996; 16: 577–84.
46. Kojiro S, Yano H, Ogasawara S, et al. Antiproliferative effects of 5-fluorouracil and interferon-alpha in combination on a hepatocellular carcinoma cell line *in vitro* and *in vivo*. J Gastroenterol Hepatol 2006; 21: 129–37.

THE JOURNAL OF BIOLOGICAL CHEMISTRY VOL. 281, NO. 52, pp. 40440–40449, December 29, 2006

YB-1 Is Important for an Early Stage Embryonic Development

NEURAL TUBE FORMATION AND CELL PROLIFERATION[*S]

Received for publication, June 21, 2006, and in revised form, October 13, 2006 Published, JBC Papers in Press, November 2, 2006, DOI 10.1074/jbc.M605948200

Takeshi Uchiumi[‡1], Abbas Fotovati[§], Takakazu Sasaguri[¶], Kohtaro Shibahara[‖], Tatsuo Shimada[**], Takao Fukuda[‖], Takanori Nakamura[‖], Hiroto Izumi[‡], Teruhisa Tsuzuki[‡‡], Michihiko Kuwano[§], and Kimitoshi Kohno[‡]

From the [‡]Department of Molecular Biology, University of Occupational and Environmental Health, School of Medicine, Yahatanishi-ku, Kitakyushu 807-8555, [§]Research Center for Innovative Cancer Therapy, Kurume University, Kurume, Fukuoka 830-0011, the [¶]Department of Pathology II, University of Occupational and Environmental Health, School of Medicine, Yahatanishi-ku, Kitakyushu 807-8555, the [‖]Department of Medical Biochemistry, Graduate School of Medical Sciences, Kyushu University, Fukuoka 812-8582, [**]Health Sciences, School of Nursing, Faculty of Medicine, Oita University, Yufushi 879-5595, and [‡‡]Medical Biophysics and Radiation Biology, Graduate School of Medical Sciences, Kyushu University, Fukuoka 812-8582, Japan

The eukaryotic Y-box-binding protein-1 (YB-1) is involved in the transcriptional and translational control of many biological processes, including cell proliferation. In clinical studies, the cellular level of YB-1 closely correlates with tumor growth and prognosis. To understand the role of YB-1 *in vivo*, especially in the developmental process, we generated YB-1 knock-out mice, which are embryonic lethal and exhibit exencephaly associated with abnormal patterns of cell proliferation within the neuroepithelium. β-Actin expression and F-actin formation were reduced in the *YB-1* null embryo and *YB-1*$^{-/-}$ mouse embryonic fibroblasts, suggesting that the neural tube defect is caused by abnormal cell morphology and actin assembly within the neuroepithelium. Fibroblasts derived from *YB-1*$^{-/-}$ embryos demonstrated reduced growth and cell density. A colony formation assay showed that *YB-1*$^{-/-}$ mouse embryonic fibroblasts failed to undergo morphological transformation and remained contact-inhibited in culture. These results demonstrate that YB-1 is involved in early mouse development, including neural tube closure and cell proliferation.

The Y-box protein family is characterized by a highly conserved cold-shock domain that binds nucleic acids and shares homology with the prokaryotic cold-shock proteins (1, 2). The human Y-box-binding gene, *YB-1*, is located on chromosome 1p34 (1). YB-1 has multiple functions but was initially identified as a transcription factor that associates with the Y-box sequence of the major histocompatibility complex class II genes (3).

YB-1 promotes cell proliferation through its transcriptional regulation of target genes such as proliferating cell nuclear antigen (PCNA),[2] epidermal growth factor receptor, DNA topoisomerase IIα, thymidine kinase, and DNA polymerase α (4, 5). We previously reported its role in the transcriptional activation of human multidrug resistance 1 (*MDR1*) and DNA topoisomerase IIα in response to various environmental stimuli (6, 7). In addition, it has been shown to chaperone RNA, modify chromatin, participate in the translational masking of mRNA, and be involved in stress responses such as the redox signaling pathway (8). Eukaryotic Y-box proteins also regulate gene expression at the translational level through their recognition of RNA (9–11), and therefore play critical roles in both mRNA turnover and translational control.

YB-1 protects mammalian cells from the cytotoxic effects induced by DNA damage. We previously reported that human cancer cell lines overexpressing YB-1 resist cisplatin, whereas the reduction of YB-1 itself leads to increased sensitivity to cisplatin, other DNA-interacting drugs, and UV irradiation (2). YB-1 is mainly localized in the cytoplasm, but translocates to the nucleus following UV irradiation of cells or treatment with anticancer drugs (12). YB-1 binds directly to repair-associated proteins such as PCNA and p53 (13), whereas proteolytic cleavage of the C-terminal fragment is linked to stress induced by DNA damage (14).

In clinical studies, the cellular level of YB-1 has been shown to correlate with tumor growth and prognosis in cancers of the ovary, lung, and breast (15). Moreover, overexpression or the nuclear presence or absence of YB-1 plays a critical role in P-glycoprotein expression, malignant progression, poor prognosis, and global drug resistance (2, 15, 16).

To understand how YB-1 proteins exert their multiple functions, we previously established mouse embryonic stem cell lines with a heterozygously targeted disruption of the *YB-1* gene (*YB-1*$^{+/-}$), and we demonstrated their hypersensitivity to cytotoxic agents such as cisplatin and mitomycin C (17).

Here we carried out targeted disruptions of the mouse *YB-1* gene to elucidate the role of YB-1 molecules *in vivo*. We show that YB-1 plays a critical role in early development in mice. The targeted disruptions were fatal in the late embryonic stage, and

*This work was supported by a grant-in-aid for scientific research on the priority area of ABC proteins, Core Research for Evolutional Science and Technology (CREST) of the Japan Science and Technology Corp. (JST), the second-term comprehensive 10-year strategy for cancer control from the Ministry of Health and Welfare of Japan, and the Cancer Research fund from Ministry of Education, Culture, Sports, Science, and Technology, Japan. The costs of publication of this article were defrayed in part by the payment of page charges. This article must therefore be hereby marked "*advertisement*" in accordance with 18 U.S.C. Section 1734 solely to indicate this fact.

[S] The on-line version of this article (available at http://www.jbc.org) contains supplemental Experimental Procedures and Figs. S1 and S2.

[1] To whom correspondence should be addressed. Tel.: 81-93-691-7423; Fax: 81-93-692-6233; E-mail: uchiumi@med.uoeh-u.ac.jp.

[2] The abbreviations used are: PCNA, proliferating cell nuclear antigen; MEF, mouse embryonic fibroblasts; PBS, phosphate-buffered saline; siRNA, small interfering RNA; FITC, fluorescein isothiocyanate; PI3K, phosphatidylinositol 3-kinase; NTD, neural tube defect; E, embryonic day; S6K, p70 S6K.

Supplemental Material can be found at: http://www.jbc.org/cgi/content/full/M605948200/DC1

TABLE 1

YB-1 deficiency causes embryonic lethality

Embryos at the indicated stages were isolated from intercrosses of heterozygous animals, and the total numbers (n) of intact as well as disintegrated or resorbed embryos were counted. For calculation of % expected (−/−): $n(-/-) \times 100 \times 3/n(+/+) + n(+/-)$.

Stage	Litters	Embryos	+/+	+/−	−/−	Abnormal (−/−)	% expected (−/−)
E10.5	15	120	27	59	34	2	118
E11.5	13	66	17	33	16	9	96
E12.5	14	82	18	48	16	16	73
E13.5	18	120	36	50	34	34	118
E14.5	12	81	18	50	13	13	57
E15.5	7	56	18	25	11	11	77
E16.5	3	17	5	9	3	3	64
E17.5	9	55	26	25	3	3	18
E18.5	3	28	5	20	1	1	12
Adult	33	185	67	118	0		0

animals showed defects in the anterior neural tube. Furthermore, we investigated the role of YB-1 in cell proliferation and the transformation activity of MEFs.

EXPERIMENTAL PROCEDURES

Animals—Animals were mated overnight, and the females were examined for a vaginal plug the following morning. Noon on the day of vaginal plug detection was recorded as day E0.5. All animal experiments were carried out according to the guidelines for animal experimentation at Kyushu University, Japan, and the University of Occupational Environmental Health, Japan. All experimental protocols were approved by the ethics committee of Kyushu University and the University of Occupational Environmental Health, Japan.

In Situ Hybridization—*In situ* hybridization of digoxygenin-labeled probes was performed as described previously (18). The digoxigenin-labeled hybridization probe was prepared from an *in vitro* transcription system (Promega, Madison, WI) using the mouse YB-1 full-length cDNA (11).

Generation of YB-1 (MSY-1)-deficient Mice—Embryonic stem cells were transfected with the linearized targeting construct that deleted exons 5 and 6 of mouse *YB-1* (*MSY-1*) (17), and recombinant clones were selected and microinjected into C57BL/6 mouse blastocytes. Chimeric males that transmitted the mutant allele to the germ line were mated with C57BL/6 females, and germ line transmission of the mutant allele was confirmed by Southern blot analysis (17). Heterozygous offspring were intercrossed to produce homozygous mutant animals. For embryo genotyping, DNA was extracted from the corresponding embryonic tissue removed from microscope sections and amplified by 30 cycles of PCR at 94 °C for 30 s, 58 °C for 30 s, and 68 °C for 1 min using the following primers: YB5-1, 5′-GGAAACCATGTGGAGATGTC, and YB3-1, 5′-GGAGGTTCAAAAGCACACTC (wild-type allele); neo5, 5′-GATTGCACGCAGGTTCTCCG, and neo3, 5′-CAAGAAGGCGATAGAAGGCG (mutant allele).

Immunohistochemistry—Cells seeded the previous day on glass coverslips were washed with phosphate-buffered saline (PBS), fixed with 3.7% formaldehyde for 30 min, rinsed twice with PBS, and then incubated with PBS containing 0.1% Triton X-100 (Sigma) for 30 min. Next, the coverslips were washed with PBS, incubated with 10% goat serum for 1 h at room temperature in a humidified container, and then incubated for 1 h with FITC-conjugated phalloidin (Sigma). After washing three times with PBS, glass slides were mounted using Slowfade mounting medium (Molecular Probes). FITC-conjugated phalloidin (Sigma) was diluted 1:200 and used to detect F-actin organization in mouse tissue and MEF cells.

Immunoblot Analysis—Embryos (E11.5) and MEF cells were lysed with radioimmunoprecipitation (RIPA) buffer (50 mM Tris-HCl, pH 7.5, 1 mM EDTA, 150 mM NaCl, 0.1% SDS, 0.5% sodium deoxycholate, and 1% Nonidet P-40) and subjected to immunoblot analysis as described previously (17) using polyclonal antibodies against YB-1 (19) and monoclonal antibodies against β-actin (AC-15; Sigma), EF-1 (Upstate, Charlottesville, VA), p70 S6K (BD Biosciences), eIF4E (BD Biosciences), Akt (9272; Cell Signaling, Danvers, MA), and PCNA (sc-56, Santa Cruz Biotechnology, Santa Cruz, CA). Band intensities were measured by Image Gauge (Fujifilm, Tokyo, Japan).

Immunohistochemical Analysis of Mouse Embryo Sections—Mouse embryo tissue was fixed with 10% buffered formalin and embedded in paraffin. Sagittal sections (5 μm thick) were cut and mounted on silane-coated glass slides. After routine deparaffination and rehydration through gradient ethanol immersions, the slides were steam-heated for 20 min to expose the antigen. Endogenous peroxidase activity was quenched using 3% (v/v) H_2O_2 followed by three 5-min washes in PBS containing 0.2% (v/v) Triton X-100, and the sections were blocked with 10% (v/v) normal goat serum in PBS. Specimens were incubated for 1 h with the YB-1 and β-actin antibody diluted in PBS containing 0.3% (v/v) Triton X-100 and 0.1% (w/v) bovine serum albumin, followed by three 5-min washes in PBS, and then incubation with the FITC-conjugated goat anti-rabbit antibody (Kirkegaard & Perry Laboratories, Gaithersburg, MD) for 30 min. Specimens were counterstained with hematoxylin for 30 s and washed with tap water. The sections were immediately dehydrated by sequential immersion in gradient ethanol and xylene, then mounted with Permount (ProSciTech, Australia), and coverslips. Images were obtained using a Leica DMRX upright microscope coupled with a digital camera (Leica, Germany).

Culture of Mouse Embryonic Fibroblasts (MEF)—Heterozygous male and female mutant mice were bred to obtain wild-type (*YB-1*$^{+/+}$), heterozygous (*YB-1*$^{+/-}$), and homozygous mutant (*YB-1*$^{-/-}$) embryos. Mouse embryonic fibroblasts were cultured in Dulbecco's modified Eagle's medium with 10% fetal bovine serum. Outgrowths were inspected daily, and their development was monitored by photography.

Proliferation Assay—Cells (1×10^4) were seeded in triplicate in 35-mm dishes and grown under high serum (10% fetal bovine

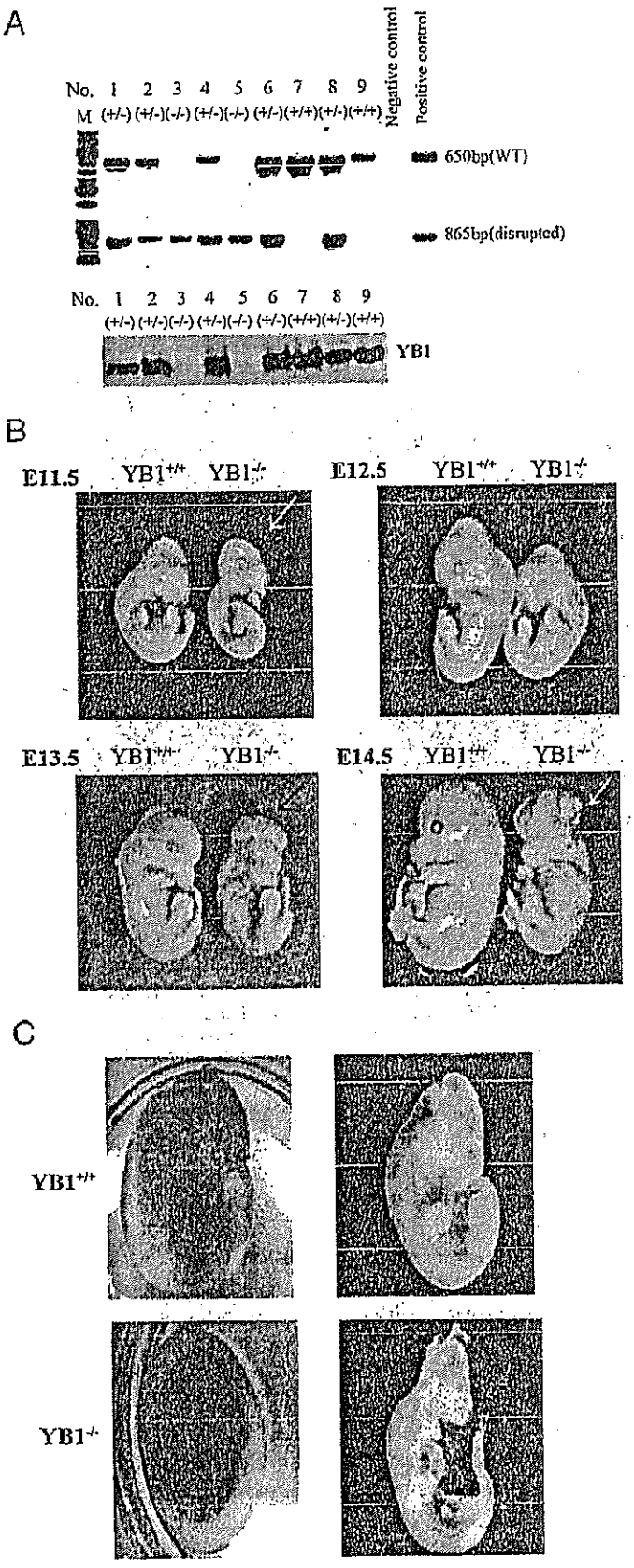

FIGURE 1. **Exencephaly in *YB-1*$^{-/-}$ embryos.** *A*, PCR genotyping of yolk sac DNA from nine E11.5 embryos. *M*, size marker. Bands of 650 bp of wild-type (*WT*) and 865 bp of mutant (*disrupted*) are shown. Total embryo protein (E11.5) was isolated, and the amount of YB-1 protein was determined by Western blotting using a polyclonal YB-1 antibody (*lower panel*). *B*, *YB-1*$^{+/+}$ and *YB-1*$^{-/-}$ embryos at E11.5 to E14.5 stages of development. Exencephaly was observed in various embryonic stages of YB-1 null mice. *Arrow* indicates brain tissue outside of the calvarium in exencephalic embryos. *C*, *YB-1*$^{+/+}$ and *YB-1*$^{-/-}$ embryos at E10.5 stage of development. *YB-1*$^{-/-}$ embryos show severe hemorrhage (*bottom left panel*) and anemia (*bottom right panel*) in comparison with wild-type embryos (*top panels*).

serum) conditions. Dishes were trypsinized and counted daily using a Coulter-type cell size analyzer (CDA-500, Sysmex, Kobe, Japan).

Transformation Assay—Cells (3×10^3) were seeded in triplicate in 10-cm dishes and maintained in Dulbecco's modified Eagle's medium supplemented with 10% fetal bovine serum and antibiotic-antimycotic (Invitrogen). Growth medium was changed every 3 days. After 14–16 days, transformation efficiency was evaluated by counting individual foci. All transformation assays were repeated at least three times. Representative plates were stained with Giemsa and photographed.

Anchorage-independent Growth—Growth in soft agar was assayed in 35-mm dishes prepared with a lower layer of 0.7% agar (Invitrogen) overlaid with top agar (0.4%) containing 5×10^3 suspended cells. Cells were fed every 3 days with media. Fifteen days after plating, colonies were stained with 2% crystal violet, and colonies with >50 cells were counted on an inverted microscope (Olympus, Tokyo, Japan).

Knockdown Analysis Using siRNA—siRNA transfections were performed according to the manufacturer's instructions (Invitrogen). Briefly, cells cultured in 35-mm dishes were transfected with stealth RNA interference-negative control duplexes and YB-1 siRNA oligonucleotides (CAACGUCGGUAUCGCCGAAACUUCA) at a final concentration of 100 μM using Lipofectamine 2000 (Invitrogen). After transfection, cell number and cell volume were quantified using an electronic sizing technique with a CDA-500 Coulter-type cell size analyzer (Sysmex). Cells were also harvested for Western blotting (17).

RESULTS

Disruption of YB-1 Causes Embryonic Lethality—To elucidate the function of YB-1 during mouse development, we used gene targeting to generate YB-1-deficient mice. Although the heterozygous offspring appeared normal and fertile (Table 1), Southern blot analysis of tail DNA from 3-week-old mice revealed that no live animals (of 144 births from heterozygote crosses) were homozygous for the *YB-1* mutation. Thus, loss of YB-1 results in embryonic lethality.

To determine the time at which the *YB-1* mutant becomes lethal, we examined embryos from *YB-1*$^{+/-}$ intercrosses at various developmental stages. PCR genotyping data of nine mouse embryos at E11.5 revealed two wild-types, five heterozygotes, and two homozygous mutants, in accordance with the expected Mendelian ratio (Fig. 1*A* and confirmed by PCR with four additional primer sets; data not shown). In contrast to wild-type embryos, the growth of *YB-1*$^{-/-}$ embryos appeared retarded as early as E10.5 (Fig. 1*B*). Most *YB-1*$^{-/-}$ embryos had been resorbed by E17.5 and *YB-1*$^{-/-}$ embryos died between E14.5 and E18.5 (Table 1). The phenotype of *YB-1*$^{-/-}$ embryos includes retarded growth, hemorrhage, and severe anemia but is otherwise normal in appearance (Fig. 1*C*).

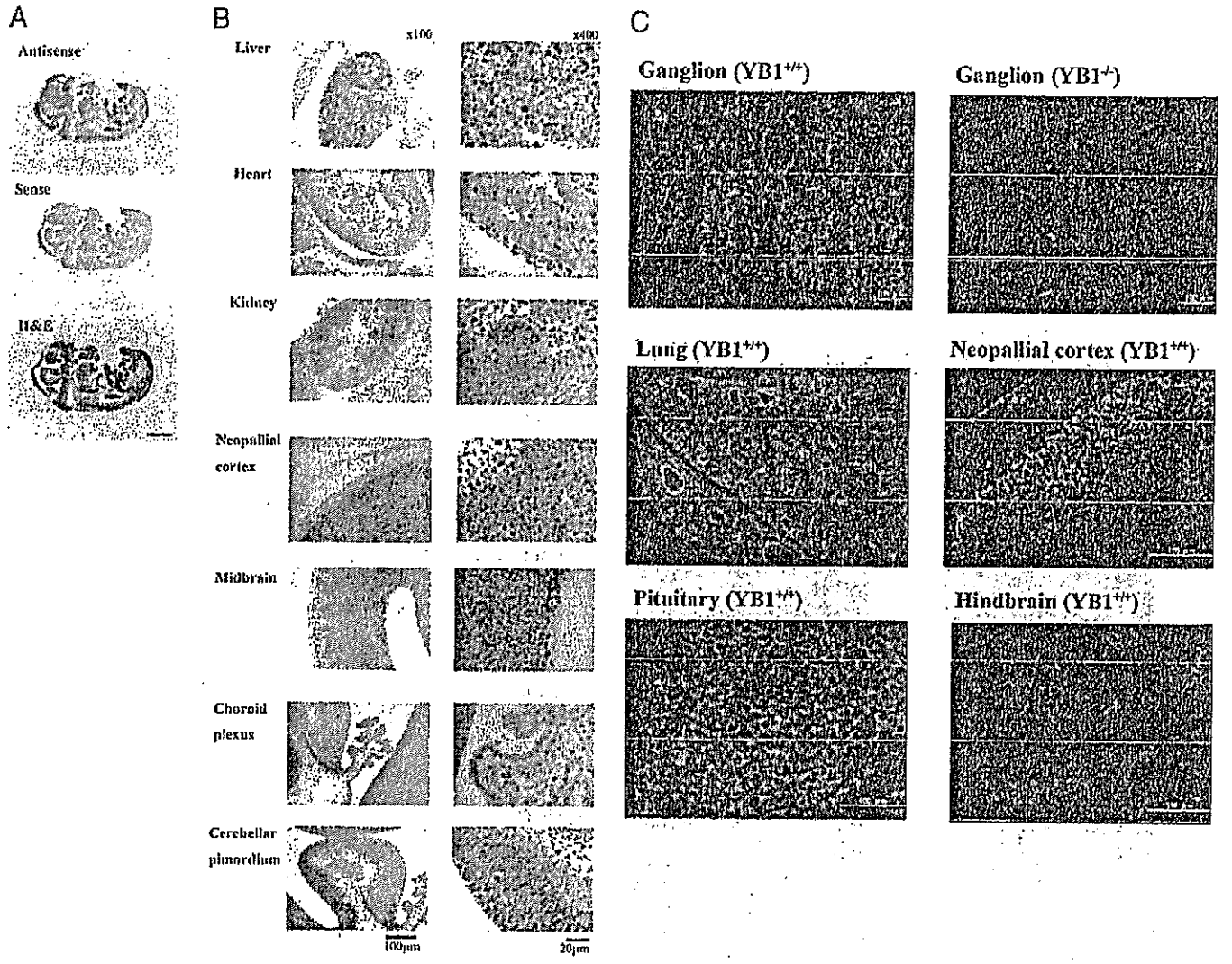

FIGURE 2. **YB-1 expression in embryonic tissues.** *A*, nonradioactive *in situ* hybridization of wild-type E13.5 mouse embryos with antisense or sense YB-1-specific probes shows that YB-1 is expressed in the whole embryo region. *Sense*, negative control; *H&E*, hematoxylin and eosin staining. *Scale bar* = 2 mm. *B*, *in situ* hybridization of wild-type E13.5 embryos showing expression of YB-1 in mouse organs. *Left panel*, *scale bar* = 100 μm. *Right panel*, *scale bar* = 20 μm. *C*, immunohistochemistry showing YB-1 expression in wild-type and YB-1 null E13.5 embryos. No staining was observed in the ganglion of the *YB-1*$^{-/-}$ mouse. *Scale bar* = 100 μm.

Mouse YB-1 Is Expressed in Most Tissues during Embryogenesis—We reported previously that human YB-1 is expressed ubiquitously in the adult (19). The YB-1 transcript and protein have also been detected in mouse embryonic stem cells (17). To determine whether the expression of mouse YB-1 is developmentally regulated, we performed *in situ* hybridization on mouse embryos tissue sections at E13.5. We found that mouse *YB-1* mRNA is expressed at whole body, specifically at high levels in the brain region (Fig. 2, *A* and *B*). Expression in the brain is widespread, with some enrichment in the cortical plate, diencephalons (thalamus), roof of the neopallial cortex, and choroid plexus extending into lateral ventricle, midbrain, and cerebellar primordium (Fig. 2*B*). *YB-1* mRNA is also strongly expressed in the posterior mesoderm, the craniofacial region, root ganglion, kidney, liver, head mesoderm, and in the developing heart (Fig. 2*B*). These data support a critical role for *YB-1* expression during embryonic development.

YB-1 protein expression in E13.5 embryos is almost ubiquitous, with high expression detected in the central nervous system, lung, kidney, and heart (Fig. 2*C*). YB-1 was predominantly localized to the cytoplasm region in wild-type embryos. No expression was detected in either connective tissues or bone of wild-type embryos and was absent from *YB-1*$^{-/-}$ embryos (Fig. 2*C*).

Neural Tube Closure Is Impaired in YB-1-deficient Mice—As shown in Fig. 1*B*, *YB-1*$^{-/-}$ embryos were smaller than their wild-type littermates, although no gross abnormalities were observed in organ or limb development. When examined at E10.5 to E13.5, ~30% of the *YB-1*$^{-/-}$ embryos exhibited exencephaly in the forebrain, midbrain, and hindbrain regions (12/80 *YB-1*$^{-/-}$ embryos) (Fig. 1*B*). Almost all of the mutant embryos were pale and anemic, as a consequence of severe blood loss through hemorrhage (seen as petechial and paintbrush patterns in Fig. 1*C*).

Histological analysis of other parts of the mutant embryos revealed that the *YB-1* mutation does not affect organogenesis, because all major organs were intact (data not shown). Exencephaly typically reflects a defect in closure of the anterior neu-

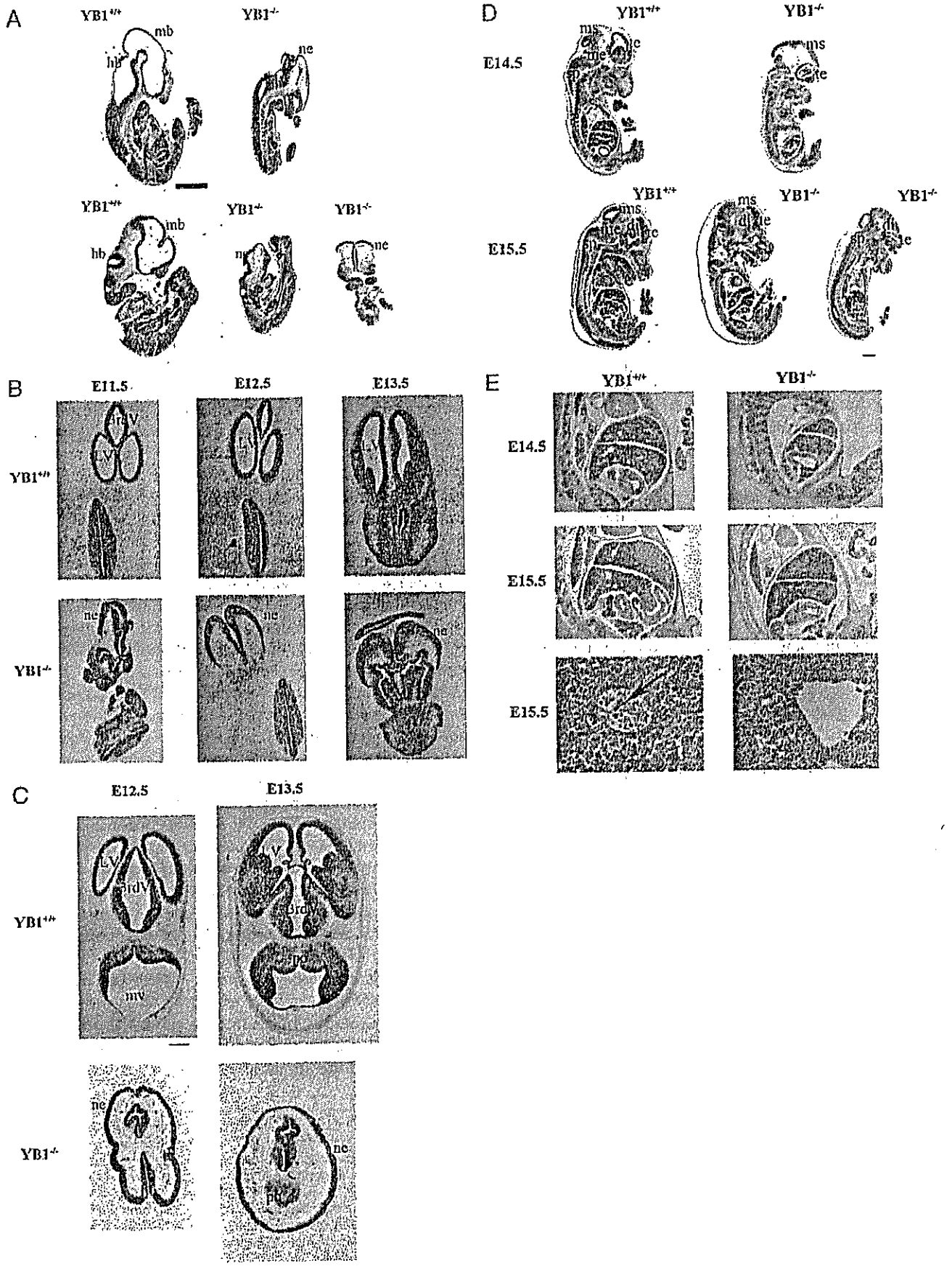

ral tube, which normally occurs between E8.5 and E9.5 (20). Fig. 3 showed a severe brain malformation characterized by exencephaly, expanded midbrain, and a disrupted cortical zone. Examination of older embryos (E13.5 to E15.5) revealed that the mutant brains failed to develop further.

Frontal and cross-sections of the hindbrain region of the E11.5 to E13.5 neural tube defect (NTD) embryos clearly demonstrate incomplete neural tube closure (Fig. 3, *B* and *C*), and the anterior neural tubes of most E10.5 to E11.5 *YB-1*$^{-/-}$ embryos failed to close with varying degrees of severity. No other cranial or neural tube abnormalities such as holoprosencephaly or impaired caudal neural closure were observed. Those *YB-1*$^{-/-}$ mice that achieved skull closure also possessed major brain structures but demonstrated retarded development of the maxilla and mandible (Fig. 3*D*). Most E15.5 *YB-1*$^{-/-}$ embryos had a subcutaneous edema of the whole body (Fig. 3*D*), which was not observed in wild-type and heterozygous mice. Moreover, fetal livers of *YB-1*$^{-/-}$ embryos were smaller than those of their *YB-1*$^{+/-}$ and *YB-1*$^{+/+}$ littermates, which is suggestive of hepatic hematopoiesis (Fig. 3*E*). *YB-1*$^{-/-}$ embryos were also anemic as a result of macroscopically detectable defects in erythropoiesis of the fetal livers (Fig. 3*E*). These data suggest that exencephaly, smaller size of organ, and severe hemorrhage account for the embryonic lethality of the *YB-1* mutation.

Enhanced EF-1 Expression in YB-1$^{-/-}$ *Embryos*—Using whole-cell extracts of eight E11.5 mouse embryos (YB-1$^{+/+}$ ($n = 1$), YB-1$^{+/-}$ ($n = 5$), and YB-1$^{-/-}$ ($n = 2$)), the expression of other proteins involved in the regulation of translation was examined by immunoblotting. Western blotting using antibodies against the YB-1 N- and C-terminal ends revealed that E11.5 *YB-1*$^{-/-}$ embryos did not express either the full-length or the truncated YB-1 protein (Fig. 4*A*; data not shown). *YB-1*$^{+/-}$ embryos expressed ~70–80% as much YB-1 as wild-type embryos. The expression of the serine/threonine protein kinase p70 S6K (S6K) was slightly reduced in *YB-1* null embryos compared with wild-type and heterozygous embryos, whereas human eukaryotic translation initiation factor 4E (eIF4E), Akt, and PCNA expression was unchanged. However, translational elongation factor-1 (EF-1) was overexpressed in *YB-1*$^{-/-}$ embryos, which might reflect a compensatory mechanism.

Decreased Proliferation in YB-1$^{-/-}$ *MEFs*—To examine the molecular basis of YB-1 in cellular proliferation, we established MEFs from wild-type ($n = 4$), *YB-1*$^{+/-}$ ($n = 4$), and *YB-1*$^{-/-}$ ($n = 4$) embryos from three independent litters at E13.5. Heterozygous MEFs (numbers 2, 56, 72, and 73) expressed approximately half as much YB-1 as wild-type MEFs, whereas *YB-1* null MEFs (numbers 3, 60, 74, and 75) expressed no YB-1. PCNA expression was comparable between all MEFs (Fig. 4*B*).

During the first three passages, cell proliferation and population doubling was comparable between *YB-1*$^{+/+}$, *YB-1*$^{+/-}$, and *YB-1*$^{-/-}$ MEFs. From passages 4 to 5 onward, all *YB-1*$^{-/-}$ MEFs analyzed showed greatly reduced proliferation and a reduction in cell numbers under base-line culture conditions (Fig. 4*C*). *YB-1*$^{+/-}$ and *YB-1*$^{+/+}$ MEFs proliferated at a similar rate. *YB-1*$^{-/-}$ MEFs exhibited premature senescence and an extended crisis as determined by an enlarged and flattened cell morphology (Fig. 5*B*). After 100 days of culture, *YB-1*$^{-/-}$ MEF cells showed reduced cell proliferation and density, which could be completely recovered to wild-type levels by expression of the YB-1 vector (Fig. 4*D*). YB-1 expression from this vector was confirmed by Western blotting (Fig. 4*B*). These data demonstrate the importance of YB-1 in cell proliferation and maintaining cell morphology.

NTD and Actin Assembly—NTDs involving mutations in genes that regulate actin arrangement at the cell membrane or play alternative roles in actin synthesis have been reported previously (21). In all cases, the defects included exencephaly caused by a failure of cranial neural fold elevation, as observed in the *YB-1*$^{-/-}$ embryos. In addition, YB-1 has been shown to associate with β-actin mRNA and the actin protein (11, 22). We used immunofluorescence to investigate whether β-actin synthesis and rearrangement are affected in E13.5 *YB-1*$^{-/-}$ embryos, and we showed that β-actin protein levels were greatly reduced in the cephalic region of the *YB-1* null embryo, in comparison with the wild type (Fig. 5*A*).

Phalloidin staining of E13.5 brain sections revealed a substantially decreased accumulation of F-actin along the basal edge of neuroepithelial cells in the null mutant embryo compared with the wild type (Fig. 5*B*). These data suggest that the reduced β-actin levels and F-actin filament formation might be responsible for the NTDs of *YB-1*$^{-/-}$ embryos. In some mutant animals, a reduced apical constriction of the neuroepithelial cells within this region was also observed.

We next examined the role of YB-1 in cell morphology and organization of the actin cytoskeleton. Wild-type MEFs had an elongated morphology and an F-actin-rich polarized cytoskeleton. In contrast, *YB-1*$^{-/-}$ MEFs were round in shape, with lower cell density (Fig. 5*B*). Most strikingly, mutant cells lacked appreciable F-actin structures such as fibers or bundles. Instead, a small amount of F-actin was seen as a fuzzy phalloidin signal that was consistently found in the subcellular region rather than in the cell perimeter (Fig. 5*B*). These results show that YB-1 is essential for organizing F-actin and maintaining the cell shape of MEFs.

As YB-1 possesses RNA binding activity and has been shown to regulate protein synthesis and mRNA stability (11, 23), we next investigated the interaction of YB-1 with β-actin mRNA.

FIGURE 3. **Neural tube defects in YB-1 mutant mice.** *A*, histological profile of sagittal sections at E10.5 showing exencephaly and defective development of cephalic area in mutant embryos. *hb*, hindbrain; *mb*, midbrain; *ne*, neuroepithelium. *Scale bar* = 1 mm. *B*, histological profile of whole E11.5–13.5 embryo frontal sections stained with hematoxylin and eosin staining showing severe disturbance of cephalic area in exencephalic embryos. YB-1$^{-/-}$ mutants exhibit open neural tubes. *Scale bar* = 200 μm. *C*, cross-sections of wild-type and *YB-1*$^{-/-}$ E12.5 to E13.5 mouse embryos showing defective neural tube closure. *YB-1*$^{-/-}$ mouse embryos were surrounded by the everted neuroectoderm of the midbrain and hindbrain. *3rdV*, third ventricle; *LV*, lateral ventricle; *mv*, mesencephalic vesicle; *po*, pons. *Scale bar* = 1 mm. *D*, sagittal sections of wild-type and *YB-1*$^{-/-}$ E14.5 to E15.5 mouse embryos showing defective neural tube closure and exencephalic phenotype of the mutant embryo (*upper right panel*). Some *YB-1*$^{-/-}$ embryos (*bottom center panels*) exhibit anterior brain structure, skull closure, and size comparable with wild-type littermates. *ms*, mesencephalon; *me*, medulla; *te*, telencephalon; *di*, diencephalon; *sp*, spinal cord. *Scale bar* = 1 mm. *E*, sagittal sections of wild-type and *YB-1*$^{-/-}$ E14.5 to E15.5 mouse embryos showing smaller liver size of the mutant embryo (*right panel*). Erythrocytes (*arrow*) are present in YB-1$^{+/+}$ liver region, but not in YB-1$^{-/-}$ liver (*lower panel*).

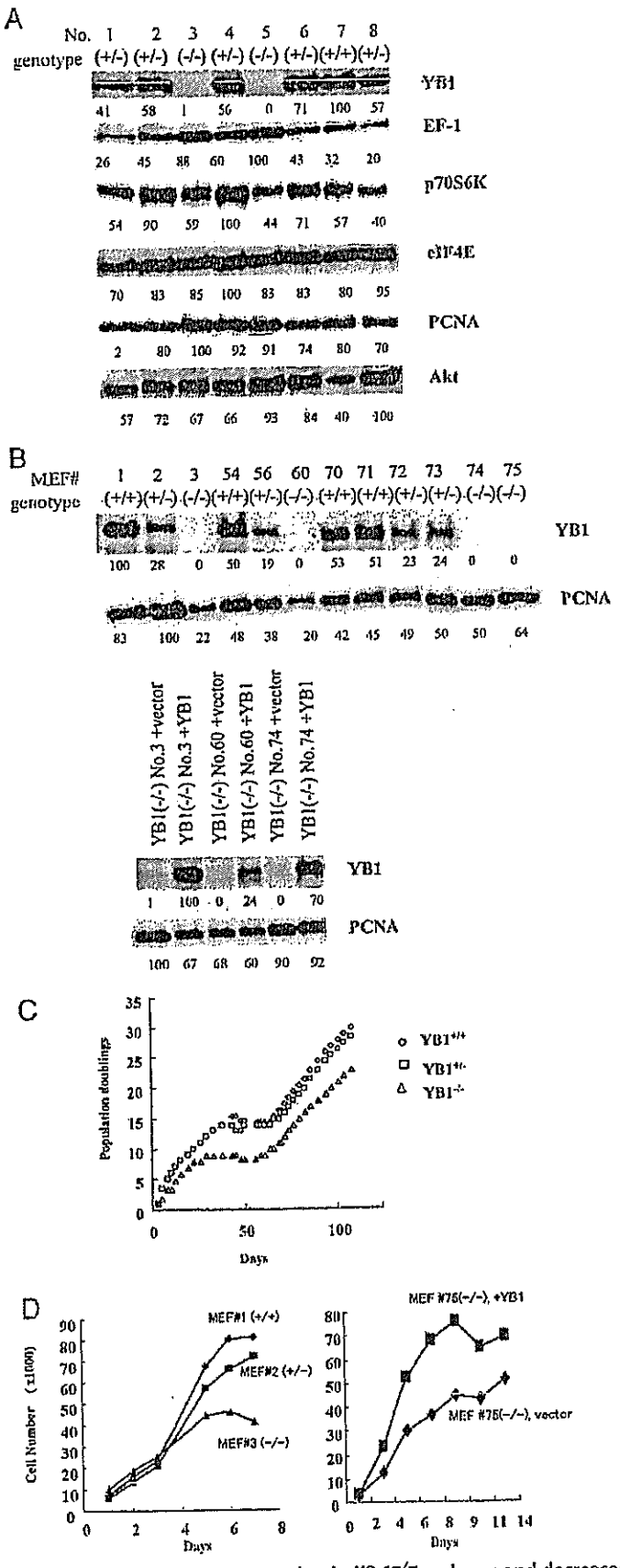

FIGURE 4. **Elevated EF-1 expression in *YB-1*$^{-/-}$ embryos and decreased growth of *YB-1*$^{-/-}$ MEFs.** *A*, Western blot analysis of protein expression in E11.5 embryonic mouse tissues. Total protein derived from eight PCR-genotyped mouse embryo tissues (50 μg of protein per lane) was immunoblotted using a specific antibody against YB-1, EF-1, p70 S6K, eIF4E, Akt, and PCNA. Elevated levels of EF-1 were observed in *YB-1*$^{-/-}$ MEFs (*lanes 3* and *5*). Relative band intensity (%) is presented. *B*, establishment of MEFs. Western blot analysis of YB-1 and PCNA expression levels after establishment of immortalized, PCR-genotyped MEF clones (*left panel*) and immortalized YB-1 null MEF clones transfected with a pIRES (control) vector or pIRES-YB-1 plasmid (*right panel*). *C*, growth curves of *YB-1*$^{+/+}$, *YB-1*$^{+/-}$, and *YB-1*$^{-/-}$ MEFs. One representative experiment is shown. Population doubling curves were determined using trypan blue exclusion. *D*, proliferation rate of MEFs as assessed by cell counts. *YB-1*$^{+/+}$ (*diamonds*), *YB-1*$^{+/-}$ (*squares*), and *YB-1*$^{-/-}$ (*triangles*) were inoculated at 5×10^4 cells/ml. The cell numbers were determined at the time points indicated. Ectopic expression of wild-type YB-1 reversed the proliferation defect (*right panel*).

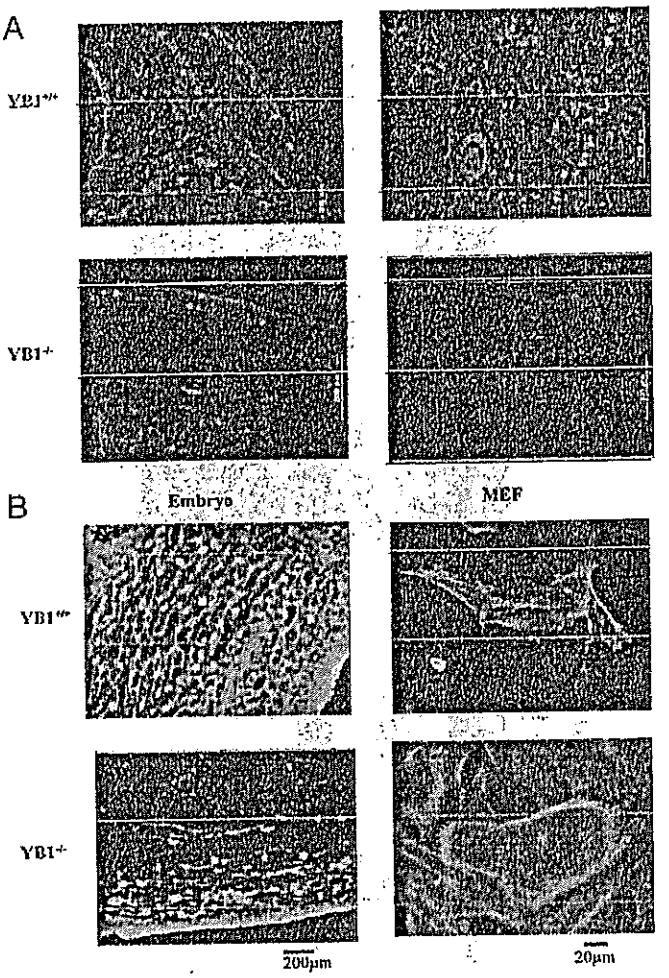

FIGURE 5. **Actin expression in the brain of wild-type and mutant embryos.** *A*, at low magnification, β-actin was shown to be ubiquitously expressed in wild-type embryos; however, *YB-1*$^{-/-}$ embryos demonstrated local reduction and derangement of β-actin expression. This is especially obvious in connective tissue-filled central nervous system supportive tissues. *B*, immunohistochemistry with FITC-phalloidin was performed in E10.5 mouse embryos (*top panels*) and MEFs (*bottom panels*). Mutant embryos showed reduced F-actin structures. Normal cytoskeletal structures can be seen in wild-type MEFs. Stress fiber formation was reduced in *YB-1*$^{-/-}$ MEFs, and cells were flatter and larger than wild-type MEFs.

An *in vitro* RNA gel shift assay was performed using purified recombinant YB-1 and a probe corresponding to full-length β-actin mRNA. Recombinant YB-1 clearly bound to β-actin mRNA, whereas the control glutathione *S*-transferase protein failed to do so (supplemental Fig. 1*A*). To determine whether the interaction occurs *in vivo*, we performed reverse transcrip-

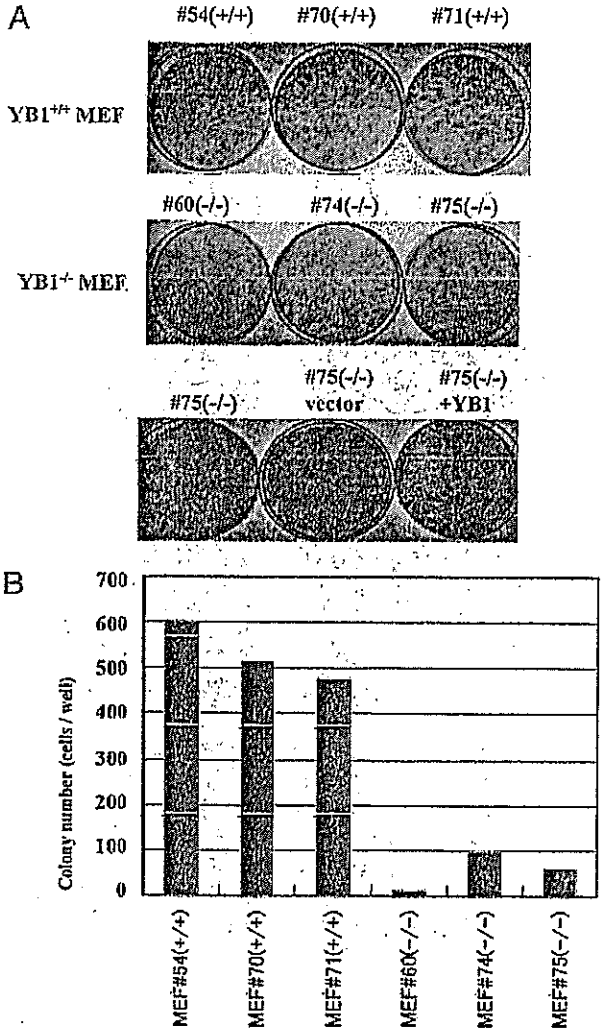

FIGURE 6. **Colony transformation activity was reduced in *YB-1*$^{-/-}$ MEFs but could be rescued by re-expression of YB-1.** *A*, three *YB-1*$^{-/-}$ MEF cell lines (*middle panel*) demonstrated reduced transformation activity compared with wild-type MEFs (*top panel*), following 2% Giemsa staining. Introduction of recombinant YB-1 restored the transformation activity (*bottom panel*). *B*, three *YB-1*$^{-/-}$ MEF cell lines demonstrated reduced colony forming activity compared with wild-type MEFs, following 2% crystal violet staining. Cells were assayed in triplicate.

tion-PCR using β-actin-specific primers on mRNA isolated by co-immunoprecipitation with YB-1. β-Actin transcript was amplified from wild-type but not from *YB-1*$^{-/-}$ MEFs (supplemental Fig. 1*B*), suggesting that YB-1 indeed interacts with β-actin mRNA in MEFs. This interaction might regulate the activity or availability of β-actin in protein synthesis.

Reduced Anchorage-independent Growth by YB-1$^{-/-}$ *Cells*—We established three wild-type and three *YB-1*$^{-/-}$ immortalized MEF lines after continuous culturing for more than 6 months to investigate their spontaneous transformation ability *in vitro*. Although the wild-type cells did not show any signs of a decrease in proliferative rate, *YB-1*$^{-/-}$ MEFs failed to undergo morphological transformation and remained contact-inhibited after 2 weeks of cultivation (Fig. 6*A*, *upper* and *middle panel*). Following re-expression of transgenic YB-1, however, the MEFs underwent morphological transformation, whereas vector-only transduced MEFs failed to do so (Fig. 6*A*, *lower panel*). Furthermore, a one-fifth reduction in anchorage-independent growth was observed in the *YB-1*$^{-/-}$ MEF clones (Fig. 6*B*).

To confirm these results, we investigated whether knockdown of endogenous YB-1 via siRNA affected cell growth and size. The siRNA oligonucleotide was directed against the YB-1 C-terminal region, with the exception of the cold-shock domain. Western blot analysis of siRNA-transfected MEFs revealed that YB-1 protein levels were reduced to 20% of wild-type levels 72 h after transfection (Fig. 7*A*). YB-1 siRNA-transfected MEFs also showed a reduced growth rate and were ~10% larger (22 μm in diameter) than the negative control transfected MEFs (20 μm in diameter) (Fig. 7, *B* and *C*). This phenomenon was consistent with our earlier observations of *YB-1*$^{-/-}$ MEFs (Fig. 5*B*) and shows that YB-1 is involved in both regulating cell growth rates and cell size. In an anchorage-independent transformation assay in soft agar, YB-1 expressing MEFs (number 70) showed morphological transformation, but siRNA-transfected MEFs demonstrated reduced transformation activity (Fig. 7*D*). These results confirm our earlier finding that YB-1 is necessary for anchorage-independent transformation activity (see also Fig. 6*A*).

DISCUSSION

This study demonstrates that YB-1 plays a critical role in DNA repair, transcription, mRNA turnover, and translational control. Previously, Lu *et al.* (24) reported that targeted disruption of *YB-1* exon 3 (encoding part of the cold-shock domain) causes embryonic lethality and showed that YB-1 is important for cellular stress responses and prevention of premature senescence after E13.5. In this study, we demonstrated that *YB-1*$^{-/-}$ embryos exhibit severe growth retardation and progressive mortality after E10.5, revealing a nonredundant role for YB-1 in early embryonic development. Our study design disrupted *YB-1* exons 5 and 6, encoding a nonspecific RNA binding region of the protein. Western blot analysis using an antibody against the YB-1 C terminus revealed that the YB-1 protein was completely absent from the E13.5 *YB-1*$^{-/-}$ embryo (Fig. 4*A*).

In this experiment, we first demonstrated that β-actin expression and F-actin formation were reduced in the *YB-1* null embryo and *YB-1*$^{-/-}$ MEF, suggesting that the neural tube defect is caused by abnormal cell morphology and actin assembly within the neuroepithelium. We also showed that *YB-1*$^{-/-}$ MEFs failed to undergo morphological transformation in culture cells and suggested that YB-1 is involved in cell proliferation.

Although only 20% of YB-1 null mutant mice showed exencephaly (Table 1), this is not an unusual finding, as mouse embryos subjected to inactivation of a critical gene via homologous recombination rarely show NTDs with complete penetrance (25). As an NTD phenotype, exencephaly reflects the failure of neural fold elevation in well defined, mechanistically distinct elevation zones (26). The genes mutated in several mouse NTD models that are involved in actin regulation (*Abl/Arg, Marcs, Mena/Profilin1, Mlp, Sprm, Vcl*) support the postulated role for actin in neural fold elevation and suggest that the NTDs are caused by an absence of the morphogenetic force normally provided by the apical redistribution of actin (25). We

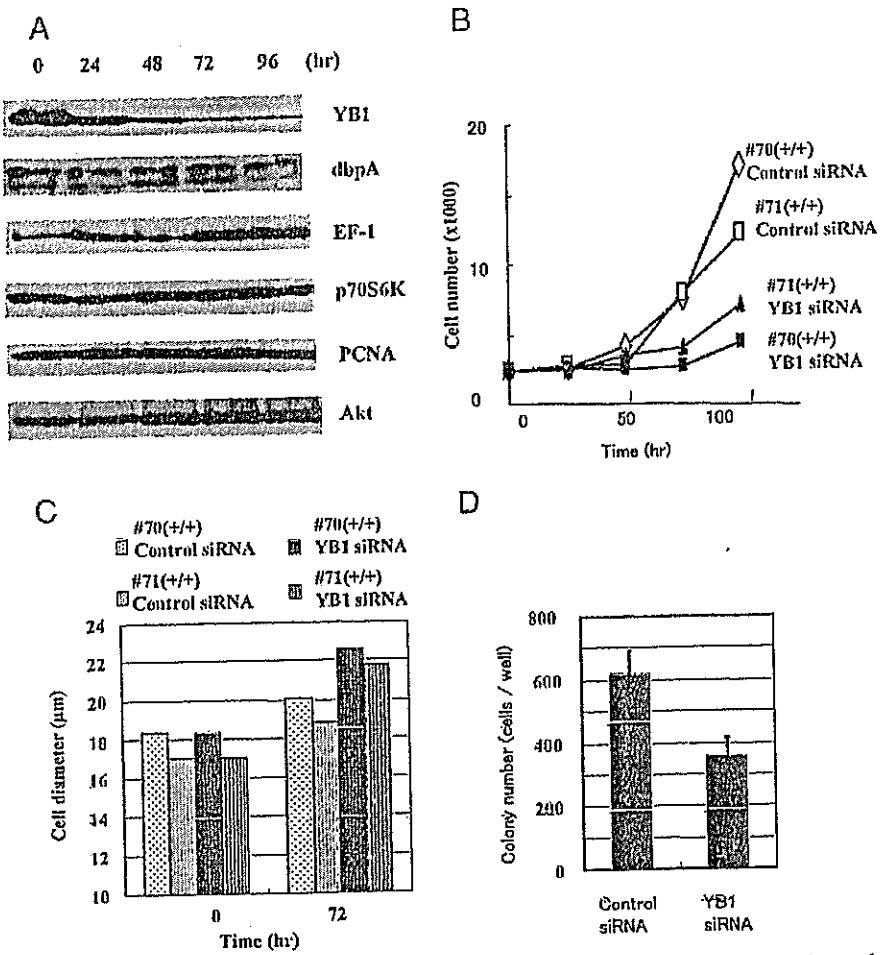

FIGURE 7. **siRNA-mediated YB-1 knockdown in MEFs.** *A*, immunoblot analysis of YB-1 siRNA-transfected MEFs. Wild-type MEFs were transfected with YB-1 siRNA, and total cell lysate (50 μg) was harvested at various time points following transfection and analyzed for indicated protein. Seventy two hours after transfection of siRNA, YB-1 protein levels had reduced by 20%. *B*, proliferation rate of siRNA-mediated MEFs. YB-1 siRNA-transfected cells demonstrated growth retardation compared with wild-type MEFs. *C*, cell size of siRNA mediated MEFs. The cell diameter of transfected MEFs was measured 0 and 72 h after transfection with a Coulter-type cell size analyzer. siRNA-transfected cells demonstrated a larger size (average diameter 22 μm) compared with wild-type cells (average diameter 20 μm). Experiments were performed in triplicate. *D*, siRNA-transfected cells demonstrated reduced colony forming activity compared with wild-type MEFs, following 2% crystal violet staining.

observed that YB-1 impairs translation of the β-actin transcript in a rabbit reticulocyte translation system (data not shown). Similar results have been reported for β-actin (27) and α-globin mRNAs (28). The strong, nonspecific *in vitro* binding of YB-1 to mRNA inhibits translation (29) and is a possible mechanism for regulating actin activity or its availability in protein synthesis. This is consistent with our finding that disruption of YB-1 leads to low β-actin levels and reduced actin assembly (Fig. 5).

Recently, the localization of β-actin mRNA to sites of active actin polymerization has been shown to modulate cell migration and neurite outgrowth (30). This localization requires the oncofetal protein Zipcode-binding protein 1 (ZBP1), which promotes translocation of the β-actin transcript to actin-rich protrusions in primary fibroblasts and neurons. ZBP1 associates with the β-actin transcript in the nucleus and prevents premature translation in the cytoplasm by blocking translation initiation. Interestingly, Matsumoto *et al.* (27) reported an interaction between YB-1 and ZBP1, suggesting that both proteins might coordinate in their regulation of β-actin mRNA localization, protection, and protein synthesis at the correct site. Further elucidation of this interaction should improve the understanding of the molecular mechanisms behind β-actin regulation.

The role of YB-1 in cell proliferation might be executed through its interaction with actin (22), as actin filaments form the contractile ring that cleaves the cell during cytokinesis (31). Alternatively, cell proliferation might be regulated by the effect of YB-1 on the cell cycle proteins cyclin A and cyclin B1, as YB-1 was found to induce strongly elevated levels of cyclin B1 protein in the mitotic stage (32). The targeted disruption of one allele of the chicken Y-box protein gene in DT40 cells results in major defects in the cell cycle (33). In this study, no difference in cyclin A and cyclin B expression was observed in *YB-1*$^{-/-}$ mouse embryos or MEFs (data not shown), suggesting that the expression level of these proteins did not cause the embryonic lethality and abnormality of the *YB-1*$^{-/-}$ mice.

Bergmann *et al.* (34) showed that transgenic mice expressing human hemagglutinin-tagged YB-1 developed diverse breast carcinomas through the induction of genetic instability caused by mitotic failure and centrosome amplification. We observed the spontaneous transformation of wild-type MEFs but showed that *YB-1*$^{-/-}$ MEFs failed to undergo morphological transformation and remained contact-inhibited (Fig. 6*B*). Re-expression of YB-1 restored the transformation activity suggesting that YB-1 is necessary for tumor promotion. Indeed, overexpression of YB-1 mRNA and protein is a hallmark of several human malignant diseases (2, 34), whereas the level of YB-1 protein expression has been linked with the prognosis of breast cancer patients and resistance to chemotherapeutic agents (5).

The nuclear translocation of YB-1 requires phosphorylation by the signal transduction protein Akt (35), which plays a role in tumor formation and progression. Evdokimova *et al.* (36) reported that phosphorylation by Akt also regulates the association of YB-1 with the capped 5′ terminus of mRNA and that activated Akt might relieve translational repression of YB-1-bound mRNA. We investigated the level of Akt protein in wild-type and siRNA-mediated YB-1 knockdown MEFs, but no difference was detected (Figs. 4*A* and 7*A*),

suggesting that YB-1 does not affect Akt protein levels in MEFs.

Target of rapamycin is a downstream kinase in the PI3K/Akt signaling pathway that phosphorylates S6K and translation initiation factor 4E-binding protein (4EBP), thus regulating translation (37). We also observed that S6K protein levels were reduced in YB-1 null mouse embryos, suggesting that YB-1 might be involved in this PI3K signaling pathway. Indeed, YB-1 is transcriptionally down-regulated in PI3K-transformed and Akt-transformed cells (29, 38). YB-1 acts downstream of the target of rapamycin, as the phosphorylation levels of S6K and 4EBP are unchanged in YB-1-overexpressing cells (39). An independent line of evidence has revealed the essential role of protein synthesis in PI3K- and Akt-induced transformation (40).

Activation of eukaryotic elongation factor 1A (eEF-1A) through phosphorylation by S6K (41, 42) enables it to bind to actin and regulate its activity or its availability in protein synthesis (43, 44). eEF-1A mutants have severe defects in cell morphology, the actin cytoskeleton, and actin bundling (44). In mammalian systems, disruption of the actin cytoskeleton results in reduced translation. In this study, we observed that YB-1 co-precipitated with eEF-1A (supplemental Fig. S2), suggesting that eEF-1A might compensate for the function of YB-1 in *YB-1*$^{-/-}$ embryos and MEFs. We also observed that another translational regulatory protein, EF-1, was overexpressed in *YB-1*$^{-/-}$ E11.5 embryos and siRNA-mediated YB-1 knockdown MEFs (Fig. 4*A* and 7*A*), indicative of an alternative compensatory mechanism.

In conclusion, we have described the function of YB-1 in the mouse embryo and in MEFs. We show that it is involved in mouse embryo development, neural tube defects, and cell proliferation.

REFERENCES

1. Makino, Y., Ohga, T., Toh, S., Koike, K., Okumura, K., Wada, M., Kuwano, M., and Kohno, K. (1996) *Nucleic Acids Res.* 24, 1873–1878
2. Kohno, K., Izumi, H., Uchiumi, T., Ashizuka, M., and Kuwano, M. (2003) *BioEssays* 25, 691–698
3. Didier, D. K., Schiffenbauer, J., Woulfe, S. L., Zacheis, M., and Schwartz, B. D. (1988) *Proc. Natl. Acad. Sci. U. S. A.* 85, 7322–7326
4. Ladomery, M., and Sommerville, J. (1995) *BioEssays* 17, 9–11
5. Kohno, K., Uchiumi, T., Niina, I., Wakasugi, T., Igarashi, T., Momii, Y., Yoshida, T., Matsuo, K., Miyamoto, N., and Izumi, H. (2005) *Eur. J. Cancer* 41, 2577–2586
6. Asakuno, K., Kohno, K., Uchiumi, T., Kubo, T., Sato, S., Isono, M., and Kuwano, M. (1994) *Biochem. Biophys. Res. Commun.* 199, 1428–1435
7. Ohga, T., Uchiumi, T., Makino, Y., Koike, K., Wada, M., Kuwano, M., and Kohno, K. (1998) *J. Biol. Chem.* 273, 5997–6000
8. Swamynathan, S. K., Nambiar, A., and Guntaka, R. V. (1998) *FASEB J.* 12, 515–522
9. Sommerville, J. (1999) *BioEssays* 21, 319–325
10. Ashizuka, M., Fukuda, T., Nakamura, T., Shirasuna, K., Iwai, K., Izumi, H., Kohno, K., Kuwano, M., and Uchiumi, T. (2002) *Mol. Cell. Biol.* 22, 6375–6383
11. Fukuda, T., Ashizuka, M., Nakamura, T., Shibahara, K., Maeda, K., Izumi, H., Kohno, K., Kuwano, M., and Uchiumi, T. (2004) *Nucleic Acids Res.* 32, 611–622
12. Koike, K., Uchiumi, T., Ohga, T., Toh, S., Wada, M., Kohno, K., and Kuwano, M. (1997) *FEBS Lett.* 417, 390–394
13. Okamoto, T., Izumi, H., Imamura, T., Takano, H., Ise, T., Uchiumi, T., Kuwano, M., and Kohno, K. (2000) *Oncogene* 19, 6194–6202
14. Sorokin, A. V., Selyutina, A. A., Skabkin, M. A., Guryanov, S. G., Nazimov, I. V., Richard, C., Th'ng, J., Yau, J., Sorensen, P. H., Ovchinnikov, L. P., and Evdokimova, V. (2005) *EMBO J.* 24, 3602–3612
15. Kuwano, M., Oda, Y., Izumi, H., Yang, S. J., Uchiumi, T., Iwamoto, Y., Toi, M., Fujii, T., Yamana, H., Kinoshita, H., Kamura, T., Tsuneyoshi, M., Yasumoto, K., and Kohno, K. (2004) *Mol. Cancer Ther.* 3, 1485–1492
16. Torigoe, T., Izumi, H., Ishiguchi, H., Yoshida, Y., Tanabe, M., Yoshida, T., Igarashi, T., Niina, I., Wakasugi, T., Imaizumi, T., Momii, Y., Kuwano, M., and Kohno, K. (2005) *Curr. Med. Chem. Anticancer Agents* 5, 15–27
17. Shibahara, K., Uchiumi, T., Fukuda, T., Kura, S., Tominaga, Y., Maehara, Y., Kohno, K., Nakabeppu, Y., Tsuzuki, T., and Kuwano, M. (2004) *Cancer Sci.* 95, 348–353
18. Yoshida, S., Ohbo, K., Takakura, A., Takebayashi, H., Okada, T., Abe, K., and Nabeshima, Y. (2001) *Dev. Biol.* 240, 517–530
19. Ohga, T., Koike, K., Ono, M., Makino, Y., Itagaki, Y., Tanimoto, M., Kuwano, M., and Kohno, K. (1996) *Cancer Res.* 56, 4224–4228
20. Fleming, A., and Copp, A. J. (2000) *Hum. Mol. Genet.* 9, 575–581
21. Harris, M. J., and Juriloff, D. M. (1999) *Teratology* 60, 292–305
22. Ruzanov, P. V., Evdokimova, V. M., Korneeva, N. L., Hershey, J. W., and Ovchinnikov, L. P. (1999) *J. Cell Sci.* 112, 3487–3496
23. Chen, C. Y., Gherzi, R., Andersen, J. S., Gaietta, G., Jurchott, K., Royer, H. D., Mann, M., and Karin, M. (2000) *Genes Dev.* 14, 1236–1248
24. Lu, Z. H., Books, J. T., and Ley, T. J. (2005) *Mol. Cell. Biol.* 25, 4625–4637
25. Juriloff, D. M., and Harris, M. J. (2000) *Hum. Mol. Genet.* 9, 993–1000
26. Harris, M. J., and Juriloff, D. M. (1997) *Teratology* 56, 177–187
27. Matsumoto, K., Tanaka, K. J., and Tsujimoto, M. (2005) *Mol. Cell. Biol.* 25, 1779–1792
28. Skabkin, M. A., Kiselyova, O. I., Chernov, K. G., Sorokin, A. V., Dubrovin, E. V., Yaminsky, I. V., Vasiliev, V. D., and Ovchinnikov, L. P. (2004) *Nucleic Acids Res.* 32, 5621–5635
29. Evdokimova, V. M., and Ovchinnikov, L. P. (1999) *Int. J. Biochem. Cell Biol.* 31, 139–149
30. Huttelmaier, S., Zenklusen, D., Lederer, M., Dictenberg, J., Lorenz, M., Meng, X., Bassell, G. J., Condeelis, J., and Singer, R. H. (2005) *Nature* 438, 512–515
31. Robinson, D. N., and Spudich, J. A. (2004) *Curr. Opin. Cell Biol.* 16, 182–188
32. Jurchott, K., Bergmann, S., Stein, U., Walther, W., Janz, M., Manni, I., Piaggio, G., Fietze, E., Dietel, M., and Royer, H. D. (2003) *J. Biol. Chem.* 278, 27988–27996
33. Swamynathan, S. K., Varma, B. R., Weber, K. T., and Guntaka, R. V. (2002) *Biochem. Biophys. Res. Commun.* 296, 451–457
34. Bergmann, S., Royer-Pokora, B., Fietze, E., Jurchott, K., Hildebrandt, B., Trost, D., Leenders, F., Claude, J. C., Theuring, F., Bargou, R., Dietel, M., and Royer, H. D. (2005) *Cancer Res.* 65, 4078–4087
35. Sutherland, B. W., Kucab, J., Wu, J., Lee, C., Cheang, M. C., Yorida, E., Turbin, D., Dedhar, S., Nelson, C., Pollak, M., Leighton Grimes, H., Miller, K., Badve, S., Huntsman, D., Blake-Gilks, C., Chen, M., Pallen, C. J., and Dunn, S. E. (2005) *Oncogene* 24, 4281–4292
36. Evdokimova, V., Ruzanov, P., Anglesio, M. S., Sorokin, A. V., Ovchinnikov, L. P., Buckley, J., Triche, T. J., Sonenberg, N., and Sorensen, P. H. (2006) *Mol. Cell. Biol.* 26, 277–292
37. Hay, N., and Sonenberg, N. (2004) *Genes Dev.* 18, 1926–1945
38. Nekrasov, M. P., Ivshina, M. P., Chernov, K. G., Kovrigina, E. A., Evdokimova, V. M., Thomas, A. A., Hershey, J. W., and Ovchinnikov, L. P. (2003) *J. Biol. Chem.* 278, 13936–13943
39. Bader, A. G., Felts, K. A., Jiang, N., Chang, H. W., and Vogt, P. K. (2003) *Proc. Natl. Acad. Sci. U. S. A.* 100, 12384–12389
40. Bader, A. G., and Vogt, P. K. (2005) *Mol. Cell. Biol.* 25, 2095–2106
41. Chang, Y. W., and Traugh, J. A. (1997) *J. Biol. Chem.* 272, 28252–28257
42. Traugh, J. A. (2001) *Prog. Mol. Subcell. Biol.* 26, 33–48
43. Edmonds, B. T., Wyckoff, J., Yeung, Y. G., Wang, Y., Stanley, E. R., Jones, J., Segall, J., and Condeelis, J. (1996) *J. Cell Sci.* 109, 2705–2714
44. Gross, S. R., and Kinzy, T. G. (2005) *Nat. Struct. Mol. Biol.* 12, 772–778

Cisplatin Resistance and Transcription Factors

Takayuki Torigoe[1], Hiroto Izumi[1], Hiroshi Ishiguchi[1], Yoichiro Yoshida[1], Mizuho Tanabe[1], Takeshi Yoshida[1], Tomonori Igarashi[1], Ichiro Niina[1], Tetsuro Wakasugi[1], Takuya Imaizumi[1], Yasutomo Momii[1], Michihiko Kuwano[2] and Kimitoshi Kohno[1,*]

[1]*Department of Molecular Biology, University of Occupational and Environmental Health, School of Medicine, Kitakyushu, Fukuoka 807-8555, Japan and* [2]*Research Center for Innovative Cancer Therapy of the 21st Century COE Program for Medical Science, Kurume University, Kurume, Fukuoka 830-0011, Japan.*

Abstract: Cisplatin is one of the most potent and widely used anti-cancer agents in the treatment of various solid tumors. However, the development of resistance to cisplatin is a major obstacle in clinical treatment. Several mechanisms are thought to be involved in cisplatin resistance, including decreased intracellular drug accumulation, increased levels of cellular thiols, increased nucleotide excision-repair activity and decreased mismatch-repair activity. In general, the molecules responsible for each mechanism are upregulated in cisplatin-resistant cells; this indicates that the transcription factors activated in response to cisplatin might play crucial roles in drug resistance. It is known that the tumor-suppressor proteins p53 and p73, and the oncoprotein c-Myc, which function as transcription factors, influence cellular sensitivity to cisplatin. So far, we have identified several transcription factors involved in cisplatin resistance, including Y-box binding protein-1 (YB-1), CCAAT-binding transcription factor 2 (CTF2), activating transcription factor 4 (ATF4), zinc-finger factor 143 (ZNF143) and mitochondrial transcription factor A (mtTFA). Two of these—YB-1 and ZNF143—lack the high-mobility group (HMG) domain and can bind preferentially to cisplatin-modified DNA in addition to HMG domain proteins or DNA repair proteins, indicating that these transcription factors may also participate in DNA repair. In this review, we summarize the mechanisms of cisplatin resistance and focus on transcription factors involved in the genomic response to cisplatin.

Key Words: ATF4, cisplatin, c-Myc, CTF2, mtTFA, p53/p73, YB-1, ZNF143.

INTRODUCTION

cis-diamminedichloroplatinum (II) (cisplatin) plays a crucial role in the treatment of many solid tumors. The mechanisms of cisplatin-induced cytotoxic activity are not completely understood; however, the therapeutic effect of cisplatin is believed to result from the formation of covalent adducts with DNA [1, 2]. Cisplatin has been shown to cause the formation of intrastrand cross-links between adjacent purines in genomic DNA. The major cisplatin cross-links are intrastrand 1, 2-d(GpG) and d(ApG); DNA damage signals then induce apoptosis in various solid tumor cells [1, 2]. Cisplatin treatment induces not only DNA damaging stress, but also oxidative and endoplasmic reticulum (ER) stresses [3, 4]. This, along with the other available evidence, demonstrates the highly complex nature of cellular sensitivity to cisplatin. Of the induced genomic responses, anti-apoptotic defenses are activated simultaneously with apoptotic signaling [5]. The major limitation to clinical treatment is the development of cisplatin resistance by tumors through these mechanisms, which include efflux and detoxification of cisplatin, and DNA repair. Other genes that are differentially expressed in association with acquired cisplatin resistance have been identified, including cytochrome oxidase I, ribosomal protein S28, elongation factor 1α, α-enolase, stathmin and HSP70 [6]. Understanding the molecular basis of cisplatin-induced genomic responses in cisplatin resistance is therefore important for determining clinical strategies.

Many genes have been identified that affect cancer cells during programmed cell death following various genotoxic stresses. The activation of the typical tumor-suppressor proteins p53 and p73 can result in cell-cycle arrest, DNA repair or apoptosis [7, 8]. Loss of p53 function confers resistance to cisplatin in various human cancer cell lines [9], whereas overexpression of p73 is associated with cisplatin resistance [10]. Recently, it has been shown that codon 72 polymorphic variants of p53 display altered mitochondrial translocation and apoptotic potential [11]. Furthermore, mutations in the *p53* gene have been widely detected in various human cancer cells, indicating that p53 might be critical in determining drug sensitivity [12]. However, it is not clear how many transcription factors play significant roles in cisplatin-induced stress responses and drug sensitivity. We believe that transcription factors for genes involved in cisplatin resistance are often activated by DNA damage; therefore, identification and characterization of cisplatin-induced transcription factors might provide a shortcut to deciphering cisplatin sensitivity and resistance in clinical treatment.

In this article, we describe the main mechanisms of cisplatin-induced apoptosis and cisplatin resistance, and discuss the transcription factors involved in resistance to

*Address correspondence to this author at the Department of Molecular Biology, University of Occupational and Environmental Health, School of Medicine, 1-1 Iseigaoka, Yahatanishi-ku, Kitakyushu, Fukuoka 807-8555, Japan; Tel: +81-93-691-7423; Fax: +81-93-692-2766;
E-mail: k-kohno@med.uoeh-u.ac.jp

1568-0118/05 $50.00+.00

cisplatin: p53/p73, c-Myc, YB-1, CTF2, ATF4, ZNF143 and mtTFA. Additionally, we refer to the potential responses of some other transcription factors, including octamer transcription factor Oct1 and the zinc-finger protein Sp1, to anti-cancer agents.

CISPLATIN-INDUCED APOPTOSIS

DNA is the primary target of cisplatin in cancer cells and one of the major cytotoxicities of cisplatin is thought to be caused by the formation of cisplatin–DNA adducts. Cisplatin binds preferentially to the N7 atom of guanine residues, especially in regions of two or more consecutive guanines. Thus, the major cisplatin cross-links are intrastrand 1, 2-d(GpG) and d(ApG), whereas the minor cross-links include intrastrand 1, 3-d(GpNpG), as shown in Fig. (1) [1, 2]. Intrastrand 1, 2-d(GpG) and d(ApG) provide the strongest basis for cisplatin-induced cytotoxicity. Cisplatin is hydrolyzed and equilibrium is maintained between cisplatin (the Cl-Cl species; $(NH_3)_2PtCl_2$), the charged species (the H_2O-Cl species; $[(NH_3)_2PtCl(H_2O)]^+$), and the neutral species (the OH-Cl species; $(NH_3)_2PtCl(OH)$) in physiological conditions of intracellular pH and chloride concentration. Charged species under low Cl^- and/or low pH conditions, such as the H_2O-Cl and H_2O-H_2O species, are more reactive than the Cl-Cl species because of their nucleophilic properties (Fig. (2)). Thus, intracellular Cl^- and pH levels could modulate the cytotoxicity of cisplatin [13].

Cisplatin can induce two major distinct apoptotic pathways via various stress signalings: the first is p53-dependent mitochondrial apoptosis, which begins with translocation of the p53-induced Bax from the cytosol to the mitochondria, followed by cytochrome *c* release and activation of caspase-9 and -3 [14]; the second is the Fas/Fas ligand-dependent caspase-8-induced apoptotic cascade [15].

Mitogen-activated protein kinase (MAPK) signaling pathways, including the extracellular signal-regulated kinase (ERK), p38 and c-Jun N-terminal kinase (JNK) pathways, play important roles in cellular responses to stress conditions, including various anti-cancer agents [16]. The ERK signaling pathway is involved in the regulation of cell growth, differentiation, proliferation and survival. By contrast, the p38 and JNK signaling pathways are stress dependent and have apoptotic regulatory functions. Cisplatin-induced activation of ERK signaling could contribute to resistance to cisplatin [17]; conversely, induction of the JNK/p38 signaling pathway in response to cisplatin induced apoptosis via Fas ligand induction in ovarian cancer cells [15]. However, Wang *et al.* have shown that ERK activation plays an important role in the cisplatin-induced apoptosis of Hela cells [3]. These results suggest that such differential effects of MAPK signals in response to drug-induction could reflect cell-type specificity. The functions of the JNK signaling pathway in apoptosis induced by cisplatin also remain unclear, as does ERK signaling [15, 18]. Further investigation is necessary to probe the exact cisplatin-induced mechanisms of these signaling pathways.

Initially, DNA damage signals induced by cisplatin can activate so-called sensor kinases. It was reported that cisplatin induces the phosphatidylinositol 3-kinase (PI3K)/AKT signaling pathway to mediate p21 expression, suggesting that it might be involved in cell-cycle regulation; however, inhibition of the PI3K/AKT pathway had no influence on sensitivity to cisplatin [19]. However, it was recently reported that AKT phosphorylates the X-linked inhibitor of apoptosis protein (XIAP) and is involved in cisplatin resistance [20]. Moreover, cisplatin could phosphorylate p53 at serine 15 and induce p53 downstream genes via activation of ataxia telangiectasia mutated and Rad3-related protein (ATR) kinase [21]. ATR signaling has also

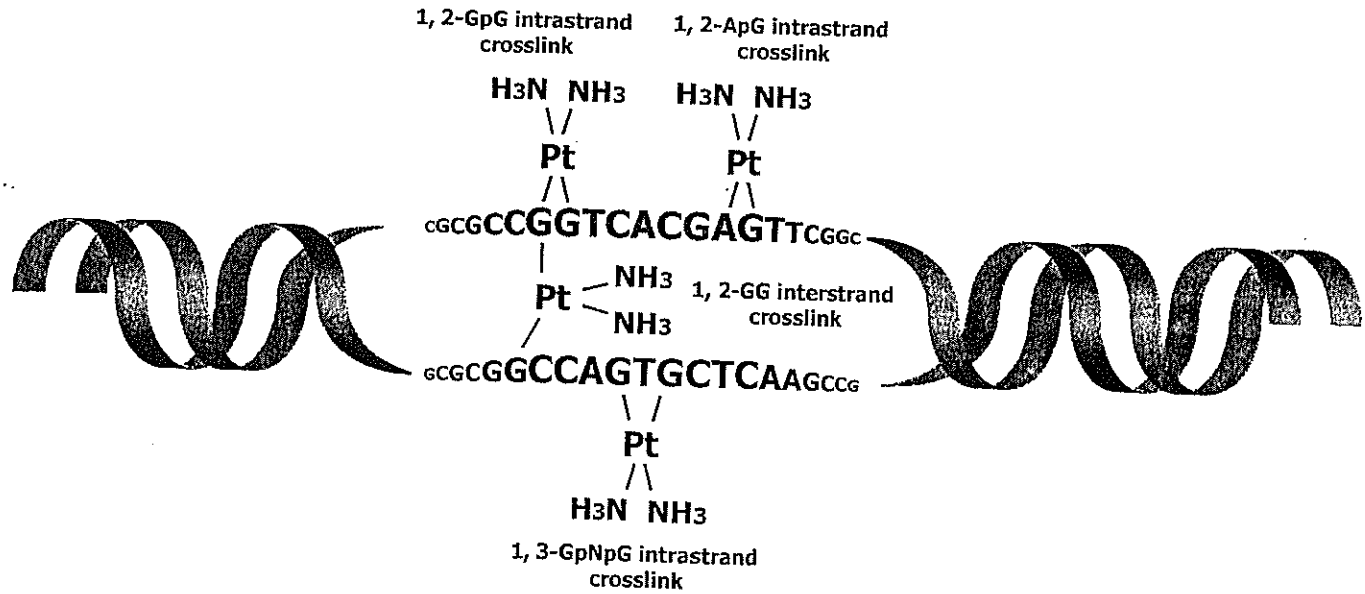

Fig. (1). Schematic diagram of cisplatin-DNA adducts.

Intrastrand 1, 2-d(GpG) and d(ApG) are the major cisplatin cross-links (85-90% of total lesions), whereas the minor cross-links is intrastrand 1, 3-d(GpNpG). The major lesions provide the strongest basis for cisplatin-induced cytotoxicity.

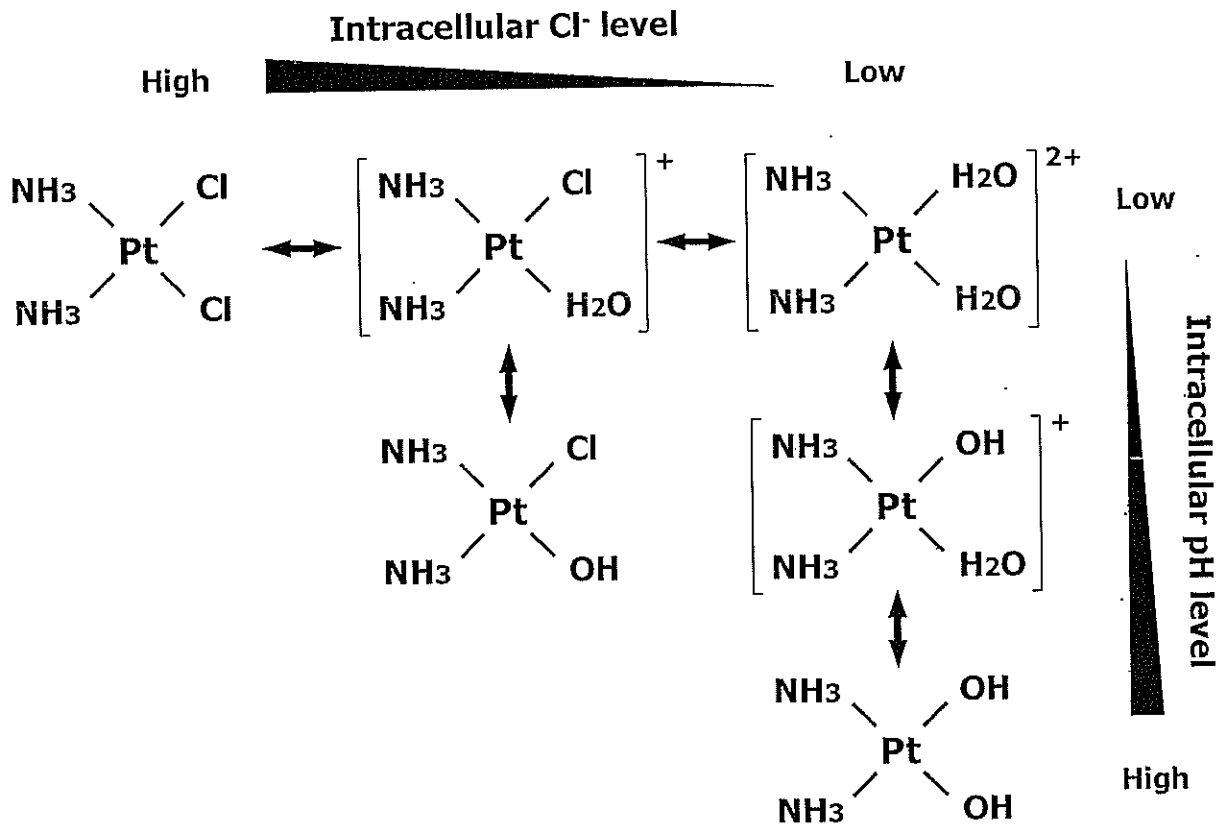

Fig. (2). Formation of intracellular cisplatin.

The equilibrium of cisplatin is affected by physiological conditions of intracellular pH and chloride concentration. The charged species under low Cl^- and/or acidic conditions (the H_2O-Cl, H_2O-OH and H_2O-H_2O species) are the most active forms.

been linked to the MAPK signaling cascade [22]. Another kinase, the c-Abl tyrosine kinase, is also activated by cisplatin. This kinase phosphorylates p73 and induces apoptosis [23]. The c-Abl pathway is also associated with the JNK signaling pathway, which is a member of the MAPK family [24]. The evidence therefore suggests that DNA damage signals might undergo crosstalk with each other.

Protein phosphatase is also involved in the cisplatin-induced signaling pathway through regulating the cellular phosphorylation state. Nuclear Src homology 2 domain-containing tyrosine phosphatase (SHP-2) was constitutively associated with c-abl and its phosphatase activity was significantly enhanced in response to DNA damage. It was reported that cells lacking SHP-2 showed markedly decreased apoptosis in response to DNA-damaging agents, such as cisplatin and γ-irradiation [25]. Furthermore, cisplatin has been shown to interact with the tumor-suppressor phosphatase and tensin homolog (PTEN), which plays an important role in cell growth and apoptosis [26]. The enzymatic activity of protein tyrosine phosphatases (PTPs) containing PTEN is often regulated by a redox system, including thioredoxin-1 [27, 28]. Apoptosis signal-regulating kinase 1 (ASK1) is a MAPK kinase kinase that activates p38 and JNK cascades, and is activated in response to oxidative stress [29]. Protein phosphatase 5 interacts with ASK1 and inhibits its activity [30]. These results provide evidence that protein phosphatase is an important modulator of apoptosis through cisplatin-induced DNA damage and oxidative stress, and that it contributes to drug sensitivity.

Reactive oxygen species (ROS) are produced upon various stress stimulations—including ultraviolet (UV) irradiation and cytotoxic agents such as cisplatin—and are closely involved in stress-induced apoptosis. ROS production can enhance sensitivity to cisplatin through activation of the JNK or p38 pathways [31], or through Fas aggregation [32]. Furthermore, it has been recently reported that cisplatin could induce apoptosis in the absence of DNA damage, through ER stress [4]. Cisplatin induced the activation of the calcium-dependent protease calpain, which activated caspase-3 and ER-specific caspase-12 in cytoplasts [4]. These data suggest that the ER might be the non-nuclear target of cisplatin.

Cisplatin-induced apoptotic pathways are complicated, as cisplatin might cause different stresses, such as DNA damaging, oxidative and ER stresses. Various cisplatin-induced stress signals can activate each pathway through specific transcription factors that act as the ultimate drug targets. Cell death or survival in response to cisplatin might be dependent on the relative intensity of, and the crosstalk between, these signal pathways. Fig. (3) shows a schematic summary of cisplatin-induced cellular signaling involved in cell death and survival. Further studies will lead to a better

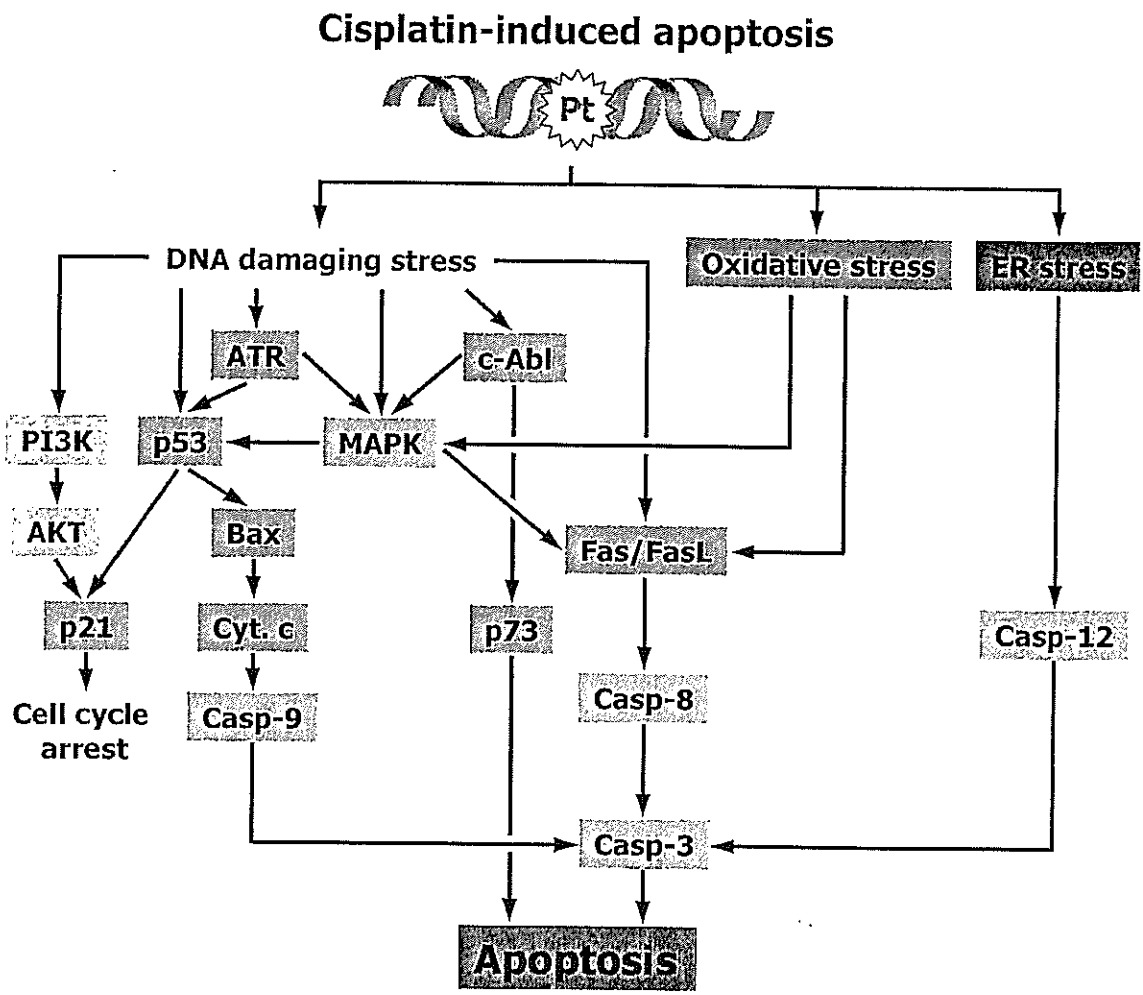

Fig. (3). Schematic summary of cisplatin-induced damaging signals.

Cisplatin induces different damaging signals, such as DNA damaging, oxidative and ER damaging stresses. These stresses can activate each pathway through specific phosphorylation cascades, which include transcription factors as the ultimate targets. The fate of cancer cells in cisplatin treatment is determined by the relative intensity of, and the crosstalk between, these signaling pathways.

understanding of the mechanisms involved in cisplatin-induced apoptosis.

MECHANISMS OF CISPLATIN RESISTANCE

The development of cisplatin resistance by tumor cells is a major clinical limitation in cancer chemotherapy. This resistance might arise due to changes in the biochemical pharmacology of cisplatin. Cisplatin resistance is induced through various mechanisms, including the reduction of cisplatin accumulation inside cancer cells [5]. One of the several possible efflux pumps for cisplatin is the multidrug resistance-associated protein 2 (MRP2; also designated cMOAT). MRP2 is a member of the MRP gene family and these ABC membrane proteins have been connected with the efflux of various drugs [33]. A recent study has shown that expression of MRP2 coincides with resistance to cisplatin [34] and Koike *et al.* have demonstrated that cisplatin sensitivity is increased by antisense MRP2 constructs [35]. These data give an insight into the relationship between MRP2 expression and drug resistance. Moreover, the copper transporters ATP7A and ATP7B have been shown to be involved in cisplatin efflux [36], and have potential as clinical markers in ovarian cancer specimens [37, 38]. However, the P-glycoprotein, which is a membrane channel encoded by the multidrug resistance 1 (*MDR1*) gene, has been reported not to participate in cisplatin resistance [39].

In another mechanism of resistance, increased activity of intracellular pathways of thiol production—including glutathione (GSH), metallothionein and thioredoxin—can contribute to the detoxification of cisplatin [5]. A small fraction of the intracellular cisplatin can bind to genomic DNA. However, a major fraction, about 60% of the intracellular cisplatin, is conjugated with GSH [40]. GSH is one of the most abundant SH-containing molecules, which can interact with cisplatin through the catalytic action of glutathione *S*-transferase π (GSTπ). GS-platinum complexes, which show inactivated cytotoxicity, are discharged from cancer cells via the glutathione conjugate export pump (GS-X pump) [1, 2]. GSTπ and γ-glutamylcysteine synthetase (γ-GCS), which is the enzyme involved in GSH biosynthesis,